Solid−Solid Phase Transformation via Internal Stress-induced Virtual Melting, Significantly below the Melting Temperature. Application to HMX Energetic Crystal

Valery I. Levitas,*,† Bryan F. Henson,‡ Laura B. Smilowitz,‡ and Blaine W. Asay‡

Center for Mechanochemistry and Synthesis of New Materials, Department of Mechanical Engineering, Texas Tech University, Lubbock, Texas 79409, and Los Alamos National Laboratory, Los Alamos, New Mexico 87545

Received: December 21, 2005; In Final Form: March 20, 2006

We theoretically predict a new phenomenon, namely, that a solid−solid phase transformation (PT) with a large transformation strain can occur via internal stress-induced virtual melting along the interface at temperatures significantly (more than 100 K) below the melting temperature. We show that the energy of elastic stresses, induced by transformation strain, increases the driving force for melting and reduces the melting temperature. Immediately after melting, stresses relax and the unstable melt solidifies. Fast solidification in a thin layer leads to nanoscale cracking which does not affect the thermodynamics or kinetics of the solid−solid transformation. Thus, virtual melting represents a new mechanism of solid−solid PT, stress relaxation, and loss of coherence at a moving solid−solid interface. It also removes the athermal interface friction and deletes the thermomechanical memory of preceding cycles of the direct-reverse transformation. It is also found that nonhydrostatic compressive internal stresses promote melting in contrast to hydrostatic pressure. Sixteen theoretical predictions are in qualitative and quantitative agreement with experiments conducted on the PTs in the energetic crystal HMX. In particular, (a) the energy of internal stresses is sufficient to reduce the melting temperature from 551 to 430 K for the δ phase during the $\beta \rightarrow \delta$ PT and from 520 to 400 K for the β phase during the $\delta \rightarrow \beta$ PT; (b) predicted activation energies for direct and reverse PTs coincide with corresponding melting energies of the β and δ phases and with the experimental values; (c) the temperature dependence of the rate constant is determined by the heat of fusion, for both direct and reverse PTs; results b and c are obtained both for overall kinetics and for interface propagation; (d) considerable nanocracking, homogeneously distributed in the transformed material, accompanies the PT, as predicted by theory; (e) the nanocracking does not change the PT thermodynamics or kinetics appreciably for the first and the second PT $\beta \leftrightarrow \delta$ cycles, as predicted by theory; (f) $\beta \leftrightarrow \delta$ PTs start at a very small driving force (in contrast to all known solid−solid transformations with large transformation strain), that is, elastic energy and athermal interface friction must be negligible; (g) $\beta \rightarrow \alpha$ and $\alpha \rightarrow \beta$ PTs, which are thermodynamically possible in the temperature range $382.4 < \theta < 430$ K and below 382.4 K, respectively, do not occur.

1. Introduction

The main geometric characteristic of a phase transformation (PT) is the transformation strain tensor ϵ^t, which transforms the unit cell of the parent phase 1 into the unit cell of the product phase 2.[1−5] For a solid−solid PT with a large ϵ^t and coherent interface, a huge amount of energy due to internal stresses can be accumulated during the PT. This energy reduces the driving force for the PT. Also, a moving interface between two solids experiences resistance due to the interaction with the stress field of crystal lattice defects such as: point defects, dislocations, as well as grain, subgrain, interface, and twin boundaries.[2−4,6−8] If the driving force for the PT (including negative contributions due to elastic energy) is smaller than the athermal (long-range) part of the resistance force *K*, which acts as dry friction, the interface will be arrested. Even if it is larger, the thermal (short-range) component of the resistance, which acts as a nonlinear viscous friction, can significantly slow the interface velocity. Elastic energy can be reduced (and the driving force can be increased) through various relaxation mechanisms, like dislocation generation and motion, twinning, and fracture.[2,3,7,8] After such a relaxation, the coherent interface is substituted with a semicoherent one, which has a larger interface energy and lower mobility. Internal stresses and the mechanism of their relaxation significantly affect the thermodynamics and kinetics of solid−solid transformation, as well as microstructure.

In this paper, we predict virtual melting as an alternative mechanism of stress relaxation and loss of coherence at a moving solid−solid interface. If melting occurs along the interface (Figure 1), then the elastic energy completely relaxes. This change in elastic energy increases the driving force for melting, reduces the melting temperature, and causes melting. Immediately after melting, stresses relax and the unstable melt (m) crystallizes in a stable phase 2. While the melt in each transforming material point exists during an extremely short time, sufficient for stress relaxation, it is nonetheless a transitional activated state rather than a real (thermodynamically stable) melt. We called this state the virtual melt, similar to virtual austenite in the theory of martensitic PT.[9] We have to note, however, that the virtual melt layer moves through the sample along with what is usually considered as a solid−solid interface; thus, it exists during the whole transformation process but at different material points. The interface between the thin

* To whom correspondence should be addressed. E-mail: valery.levitas@ttu.edu.
† Texas Tech University.
‡ Los Alamos National Laboratory.

10.1021/jp057438b CCC: $33.50
Published on Web 05/02/2006

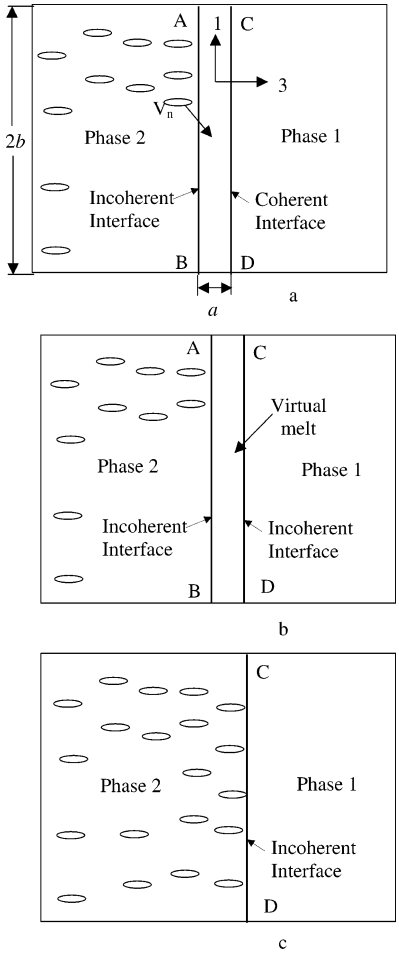

Figure 1. Scheme of the solid−solid-phase transformation $1 \rightarrow 2$ in the volume V_n via the virtual melting mechanism: (a) $1 \rightarrow 2_{\text{stressed}}$ PT occurs in a thin layer $V_n = a\Sigma$ by propagation of the coherent interface CD from the position AB; the incoherent interface AB is fixed and transforms to a grain boundary after the PT in a layer ABCD, (b) stressed phase 2 undergoes the virtual melting, and (c) solidification of the virtual melt in unstressed phase 2 which is accompanied by nanocracking.

solidified phase 2 and existing phase 2 is coherent, and because of the absence of jump in the transformation strain, it does not generate stresses. The interface between the thin solidified phase 2 and phase 1 can be completely incoherent, which does not create misfit stresses and elastic energy. Consequently, internal stress-induced virtual melting is considered as a new mechanism of the loss of coherence at the interface and relaxation of internal stresses. The liquid, as the hydrostatic medium, does not interact with the stress field of crystal defects, consequently, athermal resistance to interface propagation K is absent. One more contribution to the driving force for melting appears if the sum of the surface energy for incoherent and coherent 1−2 interfaces is larger than the sum of the phase 1−melt and phase 2−melt energies. Further consideration drives us to the conclusion that fast solidification in a thin layer leads to nanoscale cracking which, however, does not affect the thermodynamics and kinetics of the solid−solid PT. All of the above processes repeat themselves at each interface increment. It is also found that nonhydrostatic compressive stresses promote melting in contrast to hydrostatic pressure.

Our theoretical predictions are qualitatively and quantitatively confirmed by 16 experimental results[10−12] on the solid−solid PTs in the organic nitramine octahydro-1,3,5,7-tetranitro-1,3,5,7-tetrazocine (HMX) energetic crystal. In particular, it was found in refs 10 and 11 that the experimental results on kinetics of these PTs can be formally described by considering an activated state thermodynamically equivalent to the melt. The transition state free energy for $\beta \rightarrow \delta$ PT in refs 10 and 11 was found to be equal to the heat of fusion in HMX. However, it was completely unclear how the melt or liquid activated state could appear at a temperature θ, which is 120 K lower than the melting temperature of the δ phase $\theta_m = 551$ K? In fact, this experimental result motivated our current theoretical work. Also, $\beta \rightarrow \delta$ PT was observed in refs 10 and 11 at 432.6 K, just above the $\beta-\delta$ phase equilibrium temperature of 432 K.[13] This implies that the elastic energy and athermal interface friction are zero. We do not know any other solid−solid PT with large volumetric strain which does not possess the temperature hysteresis. In addition, considerable cracking, homogeneously distributed in the transformed δ phase over the several hundred nanometer scale was observed after the PT. Since the δ phase has a larger molar volume than the β phase, the δ phase is under compressive internal stresses. Thus, the origin of nanocracking was a puzzle. Finally, in the temperature range $382.4 < \theta < 435$ K, the orthorhombic α phase is stable, that is, $\beta \rightarrow \alpha$ PT is expected to occur but does not. The volumetric transformation strain for $\beta \rightarrow \alpha$ PT is two times smaller than that for the $\beta \rightarrow \delta$ PT, so there is no reason for suppression of this PT. Similarly, the $\alpha \rightarrow \beta$ and $\delta \rightarrow \alpha$ PTs do not occur in the temperature range where they are thermodynamically possible. The suggested virtual melting mechanism explains all the above and a number of other nontrivial experimental results.

The paper is organized as follows. In sections 2 and 3, various theoretical predictions are made based on the virtual melting mechanism. They are related to the thermodynamics, kinetics, and some mechanical aspects of solid−solid PTs. In section 4, numerous experimental data on the PTs in the HMX crystal are analyzed and interpreted in terms of virtual melting. Section 5 summarizes 16 experimental results on PTs in HMX crystals which qualitatively and quantitatively support the mechanism of solid−solid PTs via virtual melting. Note that the first results in this direction were published in our short letters.[14,15] Here, much more detailed theoretical and experimental justifications of the virtual melting mechanism are given.

2. Continuum Thermodynamics of Solid−Solid PT and Melting

Thermodynamic Criteria. Consider a body V with a solid−solid PT in a small region V_n bounded by an interface Σ. The transformation criterion for solid−solid PT in elastic materials, from phase 1 to phase 2, can be presented as follows[2−8]

$$F_{1\rightarrow 2} := -\Delta G V_n - \Delta(\Gamma_{1-2}\Sigma) - KV_n \geq 0 \qquad (1)$$

Here, F is the net driving force for the PT; $\Delta G V_n$ is the change in the Gibbs potential of the whole body V, which takes into account the energy of internal stresses and external forces (we use the volume V_n in this term for further convenience); Γ_{1-2} is the surface energy per unit area; symbol Δ is used for the difference between some function after and before the PT under consideration; K is the athermal dissipation due to the PT related mostly to interface friction and caused by a long-range stress field of crystal lattice defects (point defects, dislocations, as well as grain, subgrain, interface, and twin boundaries). We neglect a number of details which are not relevant to our goal. We assume stress-free external surfaces, that is, a temperature-induced PT; we neglect the change in the thermal expansion strain in comparison with the transformation strain; we neglect

the change in elastic moduli. Then eq 1 can be simplified to

$$F_{1\to 2} = -\Delta G^{e}_{1\to 2} V_n - (\Delta G_{1\to 2}(\theta) + K)V_n - \Delta(\Gamma_{1-2}\Sigma) \geq 0 \quad (2)$$

where $\Delta G^{e}_{1\to 2}$ is the change in energy of internal elastic stresses per unit transforming volume, which are caused by the transformation strain in a volume V_n, $\Delta G_{1\to 2}(\theta) = \Delta H_{1\to 2} - \theta\Delta S_{1\to 2}$ is the change in the thermal part of the Gibbs free energy per unit volume, and $\Delta H_{1\to 2}$ and $\Delta S_{1\to 2}$ are the changes in enthalpy and entropy, respectively, per unit volume. If the initial state is unstressed, then $\Delta G^{e}_{1\to 2}$ is the elastic energy of nucleus $G^{e} > 0$ and the elastic energy reduces the driving force for PT $1 \to 2$ and suppresses the PT.

As an initial configuration, we consider a plane incoherent interface AB between phases 1 and 2 with no internal stresses (Figure 1a); this is the same construction as in Figure 1c but with an interface in position AB. The plane is also a good approximation of a sufficiently short part along a curved interface. The temperature corresponds to the region of stability of phase 2, that is, $\Delta G_{1\to 2} < 0$. A PT can occur through the propagation of the incoherent interface, by an atom by atom mechanism, controlled by the energy of self-diffusion. However, adding a single atom to a flat interface significantly increases the elastic energy and reduces $F_{1\to 2}$. Thus, nucleation of a kink or ledge maybe necessary for growth, which requires additional energy. The mobility of an incoherent interface is therefore lower than that for the coherent interface, such that an alternative growth mechanism may give faster kinetics, especially at temperatures near the equilibrium transition temperature.

We therefore assume that a PT occurs in a thin layer $V_n = a\Sigma$ by fluctuational propagation of the coherent interface CD from the position AB (Figure 1). The incoherent interface AB is fixed and transforms to a grain boundary after a PT in a layer ABCD. This process can be considered a nucleation at the grain boundary (or incoherent interface). We also assume that there is no sliding along the fixed grain boundary AB, plasticity, or fracture, that is, the elastic energy does not relax and is the same as that for a coherent nucleus. For such a scenario, the change in surface energy $\Delta(\Gamma_{1-2}\Sigma) = (\Gamma_{gb} + \Gamma_c - \Gamma_{in})V_n/a$, where Γ_{gb} is the grain boundary energy, Γ_{in} is the incoherent interface energy, and Γ_c is the energy of the coherent interface. Substituting this expression in eq 2, multiplying eq 2 by V_m/V_n, and changing to molar quantities (which are designated by corresponding small letters), we obtain the PT criterion in the form

$$f^{c}_{1\to 2} = -g^{e} - \Delta g_{1\to 2}(\theta) - k - V_m(\Gamma_{gb} + \Gamma_c - \Gamma_{in})/a \geq 0 \quad (3)$$

where V_m is the molar volume and the superscript c denotes coherent.

Such a nucleation can be much faster than the incoherent interface motion when there is no barrier due to surface energy, that is, if $\Gamma_{gb} + \Gamma_c \leq \Gamma_{in}$. Energy Γ_c has the only chemical contribution, Γ_{gb} has the only structural contribution, and Γ_{in} has both contributions. Usually Γ_{in} and Γ_{gb} are comparable and are larger by 2−3 orders of magnitude than Γ_c. So, it is quite plausible that for some materials and microstructures $\Gamma_{in} \geq \Gamma_{gb} + \Gamma_c$; however, it is not necessary for our purposes.

Now we assume that the stressed phase 2 melts (Figure 1b). In a similar way, we can derive the PT criterion for melting of the internally stressed layer of phase 2

$$f_{2\to m} = g^{e} - g^{e}_{m} - \Delta g_{2\to m} - V_m \Delta\Gamma_{2-m}/a \geq 0 \quad (4)$$

where g^{e}_{m} is the energy of internal elastic stresses of the melt layer, $\Delta\Gamma_{2-m} = \Gamma_{2-m} + \Gamma_{1-m} - \Gamma_{gb} - \Gamma_c$ and Γ_{i-m} is the phase i−melt interface energy. We put $k = 0$, because liquid, as the hydrostatic medium, does not interact with the stress field of crystal defects, consequently, the resistance to interface propagation is absent. As we will show below, the elastic energy of the melt layer is negligible, that is, $g^{e}_{m} \simeq 0$. The elastic energy before melting, g^{e}, disappears after melting, thus increasing the driving force for melting. For metals $\Gamma_{i-m} = (0.3-0.45)\Gamma_{gb}$,[3] for organic crystals it is even lower, and $\Delta\Gamma_{2-m} \leq 0$, that is, there is *no barrier* for melt nucleation due to surface energy. To avoid lengthy size-dependent calculations, we put the worst-case value $\Delta\Gamma_{2-m} = 0$, decreasing the driving force for melting. This, however did not change the conclusions of the paper. It is known that allowing for $\Delta\Gamma_{2-m} \leq 0$ leads to a decrease in melting temperature by several degrees (premelting).[16]

From the phase equilibrium condition $f_{2\to m} = 0$, one determines how the melting temperature θ_m reduces as a result of elastic energy of solid phase 2

$$\theta^{e}_{m} = (\Delta h_{2\to m}(\theta^{e}_{m}) - g^{e})/\Delta s_{2\to m}(\theta^{e}_{m}) \quad (5)$$

Generally, because the change in enthalpy $\Delta h_{2\to m}$ and entropy $\Delta s_{2\to m}$ are functions of temperature, eq 5 is a nonlinear equation with respect to θ^{e}_{m}. The smaller $\Delta s_{2\to m}$ is and the larger g^{e} is, the larger $\theta_m - \theta^{e}_{m}$ is. Note that we use bulk thermodynamic functions for the thin liquid layer; previous works on surface premelting and quasi-liquid formation[16] support this.

Internal Stresses and Their Elastic Energy. Let us estimate g^{e}. We will consider a transforming volume V_n as a penny-shaped ellipsoid with axes a and b and an aspect ratio $n = a/b \ll 1$. This will model plane interface propagation and will allow us to use the well-known Eshelby solution for internal stresses and elastic energy.[17] We choose a Cartesian coordinate system with axis 3 normal to the interface and axes 1 and 2 in the interface; see Figure 1a. The components σ_{ij} of the stress tensor due to the components of the transformation strain tensor ϵ^{t}_{ij}, i, $j = 1$, 2, and 3, in the volume V_n in isotropic approximation are[17]

$$\frac{\sigma_{11}}{2\mu} = \frac{-\nu}{1-\nu}(\epsilon^{t}_{11} + \epsilon^{t}_{22}) - \epsilon^{t}_{11} + n\frac{\pi}{32(1-\nu)}(13\epsilon^{t}_{11} + (16\nu - 1)\epsilon^{t}_{22} - 4(2\nu + 1)\epsilon^{t}_{33})$$

$$\frac{\sigma_{22}}{2\mu} = \frac{-\nu}{1-\nu}(\epsilon^{t}_{11} + \epsilon^{t}_{22}) - \epsilon^{t}_{22} + n\frac{\pi}{32(1-\nu)}((16\nu - 1)\epsilon^{t}_{11} + 13\epsilon^{t}_{22} - 4(2\nu + 1)\epsilon^{t}_{33})$$

$$\frac{\sigma_{33}}{2\mu} = -n\frac{\pi}{8(1-\nu)}((2\nu + 1)(\epsilon^{t}_{11} + \epsilon^{t}_{22}) + 2\epsilon^{t}_{33})$$

$$\frac{\sigma_{23}}{2\mu} = n\frac{\pi(\nu - 2)}{4(1-\nu)}\epsilon^{t}_{23}$$

$$\frac{\sigma_{31}}{2\mu} = n\frac{\pi(\nu - 2)}{4(1-\nu)}\epsilon^{t}_{31}$$

$$\frac{\sigma_{12}}{2\mu} = -\epsilon^{t}_{12} + n\frac{\pi(7 - 8\nu)}{16(1-\nu)}\epsilon^{t}_{12} \quad (6)$$

where μ is the shear modulus and ν is Poisson's ratio. The elastic energy per unit volume of the nucleus can be determined as $G^{e} = -0.5\sum_{i=1}^{3}\sum_{j=1}^{3}\sigma_{ij}\epsilon^{t}_{ij}$.[17] If we neglect all terms containing n

$\ll 1$ in eq 6, then we receive for the elastic energy per mole $g^e = V_m G^e$

$$g^e = V_m \mu((\epsilon_{11}^t)^2 + (\epsilon_{22}^t)^2 + 2\nu\epsilon_{11}^t \epsilon_{22}^t + 2(1-\nu)(\epsilon_{12}^t)^2)/(1-\nu) \quad (7)$$

Neglecting terms with $n \ll 1$ is equivalent to considering V_n as an infinite layer. In this case, nonzero transformation strains in the interface plane ϵ_{11}^t, ϵ_{22}^t, and ϵ_{12}^t only produce nonzero stresses in the interface plane σ_{11}^t, σ_{22}^t, and σ_{12}^t. It is noteworthy that for a negligible n, eq 6 exactly coincides with Hooke's law, if we substitute transformation strain with elastic strain ϵ_e and change the sign. Consequently, the transformation strain is completely compensated for by the elastic strain and the total strain in the volume V_n is $\epsilon = \epsilon_e + \epsilon_t = 0$. Because neither tractions nor displacements are present at the interfaces, the remaining part $V - V_n$ of the body of volume V is uncoupled from the interface and is stress free. The whole elastic energy is concentrated in the transforming layer.

Let us determine the energy of elastic stresses in a melt of phase 2. After melting, the volumetric transformation strain $\epsilon_0^m = \epsilon_{11}^m + \epsilon_{22}^m + \epsilon_{33}^m$ with respect to the parent phase 1 is prescribed and the stress tensor reduces to hydrostatic pressure. The interface is incoherent after melting. All components of the transformation strain and pressure can be formally found from eq 6 using the following procedure for incoherent inclusion.[17] First, we make all shear transformation strains and consequently stresses identically zero. Second, we chose such transformation strains ϵ_{11}^m and ϵ_{22}^m which reduce the stress state to a hydrostatic one. We can consider $\epsilon_{11}^m = \epsilon_{22}^m$ (this does not change the final result) and $\epsilon_{33}^m = \epsilon_0^m - 2\epsilon_{11}^m$. By substituting these expressions in eq 6 for the normal stresses, we find from the condition $\sigma_{22} = \sigma_{33}$ (or $\sigma_{11} = \sigma_{33}$) the transformation strain in the melt with respect to phase 1

$$\epsilon_{22}^m = \frac{n\epsilon_0^m \pi(1-2\nu)}{8(1+\nu) - 3n\pi(1+4\nu)}$$

$$\epsilon_{33}^m = \epsilon_0^m - \frac{2n\epsilon_0^m \pi(1-2\nu)}{8(1+\nu) - 3n\pi(1+4\nu)} \simeq \epsilon_0^m \quad (8)$$

The substitution of this expression in eq 6 for any normal stress results in a final expression for the pressure in the melt

$$p = -\sigma_{ii} = 2\mu n \epsilon_0^m \frac{\pi(1+\nu)(2 - n\pi(1+\nu))}{(1-\nu)(8(1+\nu) - 3\pi n(1+4\nu))} \quad (9)$$

The elastic energy of the melted inclusion per mole is

$$g_e^m = 0.5 V_m p \epsilon_0^m = V_m \mu n (\epsilon_0^m)^2 \frac{\pi(1+\nu)(2 - n\pi(1+\nu))}{(1-\nu)(8(1+\nu) - 3\pi n(1+4\nu))} \quad (10)$$

As this energy is proportional to n, it is negligible in comparison with g^e; this was taken into account in eq 5.

Note that for tensile $\epsilon_{ii}^t > 0$ (like for $\beta \rightarrow \delta$ PT), compressive stresses in V_n are generated after $1 \rightarrow 2$ PT. In most cases, melting is accompanied by volumetric expansion $\epsilon_0^m > 0$ (in particular, for $\beta \rightarrow \delta$ PT) and the melt temperature is observed to increase with increasing pressure. This seems to contradict our results. The solution is in the nonhydrostatic stresses and transformation strains, as well as in the difference between external and internal stresses. According to eq 8, the transformation strains along the interface with respect to phase 2 for melting are $\epsilon_{ii}^m = n\epsilon_0^m \pi(1-2\nu)/(8(1+\nu)) - \epsilon_{ii}^t$ (here, $i = 1, 2$). Thus, the transformation strains ϵ_{11}^m and ϵ_{22}^m along the interface in the liquid with respect to phase 1 are proportional to n and consequently are smaller than the same transformation strains in phase 2. This implies $\epsilon_{ii}^m < 0$, that is, during melting, compression occurs along the interface and compressive stresses σ_{11} and σ_{22} promote melting. Orthogonal to the interface direction, the transformation strain during melting is of course tensile and is even larger than ϵ_0^m. However, stress σ_{33} before melting is proportional to n and is negligible in comparison with σ_{11} and σ_{22} (see eq 6).

It is easy to show the difference between the effect of external and internal pressure. Prescribed external pressure p_{ext} makes a contribution to the driving force for the PT in the form $-V_m p_{ext} \epsilon_0^t$, which depends on the sign of ϵ_0^t. Internal stresses are determined by transformation strains rather than by prescription, and as follows from eq 7, the elastic energy of internal stresses is always positive and if ϵ_{11}^t and ϵ_{22}^t have the same sign, it is independent of the sign of the transformation strains. Thus, the same consideration can be repeated for the reverse PT, in particular for the $\delta \rightarrow \beta$ PT.

Solidification and Nanocracking. After melting, internal stresses relax and the unstressed melt is unstable with respect to solid phase 2 (Figure 1c), because for $\theta_m^e < \theta_m$, $f_{m\rightarrow 2} = -\Delta g_{m\rightarrow 2} > 0$. We assume that during solidification of a thin liquid layer, the layer has a complete adhesion to the solid phases. The solidification then generates compressive equiaxial transformation strains $\epsilon_{ii}^s = \epsilon_0^s/3 < 0$, where $i = 1$, 2, or 3 and ϵ_0^s is the volumetric transformation strain during solidification. Substituting this ϵ_{ii}^s in eq 6 and neglecting the terms with n, one obtains $\sigma_{11} = \sigma_{22} = -2\mu\epsilon_0^s(1+\nu)/(3(1-\nu)) = -E\epsilon_0^s/(3(1-\nu))$, where E is Young's modulus and the relationship $2\mu(1+\nu) = E$ was used; all other stresses are zero. In the elastic regime, these tensile stresses would cause tensile elastic strains $\epsilon_{11}^e = \epsilon_{22}^e = \sigma_{11}(1-\nu)/E = -\epsilon_{11}^s$ and compressive elastic strain $\epsilon_{33}^e = -2\nu\sigma_{11}/E$. During solidification, the yield stress and the maximal normal tensile stress (resistance to fracture) are negligible. Thus, we assume that the elastic strains ϵ_{11}^e and ϵ_{22}^e completely relax through one or more of these mechanisms (Figure 1c): vacancy generation, nanocracking, cavitation, or the unstable plastic flow leading to microvoid formation (like in the neck of a tensile specimen before macroscopic fracture), that is, the inelastic strain due to cracking is $\epsilon_{11}^c = \epsilon_{22}^c = \epsilon_{11}^e = -\epsilon_{11}^s$. This will lead to the complete relaxation of stresses σ_{11} and σ_{22} and consequently the compressive strain ϵ_{33}^e. The volumetric strain due to cracking $\epsilon_0^c = 2\epsilon_{11}^c = -2\epsilon_0^s/3 > 0$, which is the upper bound for the porosity induced by this mechanism. The characteristic size of the initial microcavities has the order of magnitude of a, that is, of nanometer size. However, as cracking occurs sequentially in the whole transforming volume, the size can grow by diffusion and coalescence, if the temperature is high enough.

Let us consider now an interface between the nanocracked phase 2 and noncracked phase 2, which made a small incremental advance as in Figure 1. If $\epsilon_t > 0$, then the transforming layer will be under compression due to displacement continuity at the coherent 1−2 phase interface. Cracks cannot propagate in a compressed layer. They will be partially closed in the vicinity of the interface between cracked and noncracked material. However, because stresses outside the transforming layer are small, the closure will not be significant, nor will stress

reduction in the transforming layer. When the transforming layer melts, some melt atoms can penetrate into the nanocracks and prevent their closure during solidification. Then, the next interface advance starts with the same initial state as it was described above. It follows from the above discussion that for $\epsilon_t > 0$ nanocracking cannot appear without the virtual melting.

If $\epsilon_t < 0$, then the transforming layer will be under tension due to the displacement continuity at the coherent 1−2 phase interface. Cracks, in principle, can propagate in a transforming layer without virtual melting. This will reduce internal stresses and their energy g^e only in some regions surrounding the crack, roughly in the region of a but not between the cracks where the interface is coherent. The sum of the elastic and surface energy of such a layer may be (but is not necessarily) even larger than before cracking, because the stress concentrator at the crack tips moved from the previously transformed layer to the transforming layer. Thus, cracking due to solid−solid PT (rather than due to solidification) does not prevent virtual melting. For tensile stresses, in addition to the propagation of the existing cracks, crack nucleation is also possible in the direction orthogonal to tensile stresses. However, if a is smaller than the critical crack length under a given stress field, then the crack cannot nucleate. Thus, even for compressive $\epsilon_t < 0$ during the solid−solid PT, when partial internal stress relaxation due to cracking is possible, virtual melting may still take place and will lead to complete stress relaxation. Cracks which appeared during the solid−solid PT will disappear during the virtual melting and new nanocracks will appear during the solidification.

Let us consider plasticity as a stress relaxation mechanism. From strained epitaxial film research, we know that dislocation nucleates at some critical width of the films when critical stored energy is accumulated.[18] For some systems, melting can occur at smaller thicknesses. The appearance of dislocation decreases the total elastic energy of the layer but increases local elastic energy in the small vicinity of dislocation which promotes the nucleation of the melt. In organic materials with complex molecules and relatively large cell parameters (like HMX), nucleation of dislocation is naturally suppressed as a result of their high energy.

If virtual melting cannot occur at a given temperature and plasticity is suppressed, then cracking is the main mechanism of the elastic energy release.

It follows from the theory of PT in inelastic materials[7] (which includes dislocation plasticity and fracture) that the inelastic process of the appearance of microcavities does not contribute to the driving force for the 1 → 2 PT directly, only though stress variation. As the stresses before and after 1 → 2 PT are zero, the stress (and elastic energy) change is zero as well. Each inelastic process has its own driving force independent of the driving force for the PT. In the given case, internal stresses cause damage when resistance to damage is close to zero. Consequently, the appearance of microcavities does not affect the driving force for the 1 → 2 PT, which is a nontrivial result. After solidification, the initial incoherent interface AB disappears and CD transforms to a new incoherent 1−2 interface, that is, we arrived at the same configuration as we started from but with the incoherent 1−2 interface shifted from position AB to CD. Then the same processes can be repeated at the next interface increment.

3. Kinetics

Without virtual melting, the elastic energy and change in surface energy (if positive) reduce the driving force $f_{1\to2}$ PT

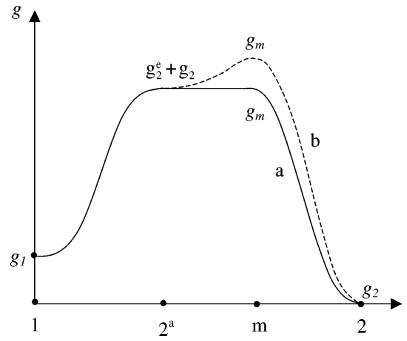

Figure 2. Change in the Gibbs energy along the transformation path 1 → 2 through elastically stressed phase 2^a and virtual melt m which are transitional activated states: (a) when $g^e + g_2 = g_m$ and melting occurs due to fulfillment of the thermodynamic melting criterion and (b) when $g^e + g_2 < g_m$ and melting occurs as a thermally activated nucleation.

(see eq 3). For the complex transformation process $1 \to 2_{stressed} \to$ virtual melt $\to 2_{relaxed}$, the net driving force is

$$f^m_{1\to2} = -\Delta g_{1\to2} = -(\Delta h_{1\to2} - \theta \Delta s_{1\to2}) \qquad (11)$$

where the elastically stressed coherent phase 2 and melt are activated states (Figure 2). There is no change in the interface energy in the expression for the driving force $f^m_{1\to2}$, because this would simply result in the incoherent interface AB shifting to a new position CD. We did not include k in eq 11, because the coherent phase 2 activated state is not supposed to be subjected to dry interface friction. Note that the nanocracking of phase 2 reduces the effective elastic moduli and the actual volume of the solid phase slightly but increases the surface energy. In eq 11, we neglect the contribution of nanocracking to the Gibbs energy.

The interface velocity for negligible k can be presented in the form

$$v = v_0\left(\exp\left(-\frac{E_{1\to2}}{R\theta}\right) - \exp\left(-\frac{E_{2\to1}}{R\theta}\right)\right) \qquad (12)$$

where v_0 is the preexponential factor, $E_{1\to2}$ and $E_{2\to1}$ are the activation energies for 1 → 2 and 2 → 1 PTs, respectively, and R is the gas constant. As the simplest case, we assume that the changes in surface energy during nucleation of the stressed coherent phase 2 and virtual melting are negligible in eqs 3 and 4 (the opposite case for eq 3 will be considered below). According to Figure 2a, $E_{1\to2} = g_2^e + \Delta g_{1\to2}$ and $E_{2\to1} = g_2^e$. An important point in our kinetic analysis is a barrierless melting ($\Delta\Gamma_{2-m} \le 0$). If this were not the case, then one would have to consider a critical melt nucleus and multiply an activation energy by the number of moles in the nucleus. This will make the virtual melting mechanism kinetically improbable. Also, the activation energy would not be equal to the melting energy, and this is inconsistent with our observations.[10,11]

The condition that the melting occurs under phase equilibrium $f_{2\to m} = 0$ results in $g_2^e = \Delta g_{2\to m}$ (see eq 4). Then both activation energies

$$E_{1\to2} = \Delta g_{2\to m} + \Delta g_{1\to2} = \Delta g_{1\to m}$$

and

$$E_{2\to1} = \Delta g_{2\to m} \qquad (13)$$

coincide with the corresponding change in the Gibbs potential during melting of phases 1 and 2. Substitution of eq 13 in eq

12 results in

$$\upsilon = \upsilon_0 \exp\left(-\frac{\Delta g_{2\to m}}{R\theta}\right)\left[\exp\left(-\frac{\Delta g_{1\to 2}}{R\theta}\right) - 1\right] = \upsilon_0 \exp\left(\frac{\Delta s_{2\to m}}{R}\right)\exp\left(-\frac{\Delta h_{2\to m}}{R\theta}\right)\left[\exp\left(-\frac{\Delta g_{1\to 2}}{R\theta}\right) - 1\right] \quad (14)$$

The term in square parentheses is a function of the driving force for $1 \to 2$ PT, which is equal to zero for thermodynamic equilibrium and greater (smaller) than zero in the region of stability of the second (first) phase. The temperature dependence of the rate constant is determined by the heat of fusion $h_{2\to m}$. The rate of change of concentration of the second phase, $\dot{c}$, can be determined by the equation

$$\dot{c} = \int_\Sigma \upsilon d\Sigma/V = \upsilon_{av}\Sigma/V \quad (15)$$

where Σ is the total 1−2 phase interface area and υ_{av} is the interface velocity averaged over Σ. The total interface area depends on the geometry of propagating interfaces. For example, if the interface propagates from one end to the other of the cylindrical sample and is orthogonal to the sample axis, then Σ = const during the entire propagation and has jumps from zero to Σ and from Σ to zero at the beginning and the end of transformation, respectively. If there are numerous interfaces of stochastic geometry, then in the first approximation $\Sigma \sim c(1 - c)$. This equation at least satisfies two limit cases that $\Sigma = 0$ when $c = 0$ or $c = 1$. Assuming that υ_{av} can be determined by the eq 13, we obtain

$$\dot{c} = b\upsilon c(1-c) = c_0 c(1-c)\exp\left(-\frac{\Delta h_{2\to m}}{R\theta}\right)\left[\exp\left(-\frac{\Delta g_{1\to 2}}{R\theta}\right) - 1\right] \quad (16)$$

where b and c_0 are the parameters to be determined experimentally.

Even if elastic energy g^e is not sufficient for the melting (i.e., $f_{2\to m} < 0$), the corresponding difference in Gibbs energy will represent the activation energy for melting. Then, according to Figure 2a, again eq 13 in eq 14 is valid. An important point is that the activated liquid state exists long enough for the relaxation of stresses, which leads to the transition to phase 2 rather than back to phase 1.

It is known that the components of the transformation strain tensor ϵ_t and consequently, internal stresses and their energy g^e (see eqs 6 and 7) depend on the mutual orientation of the crystal lattices of the phases 1 and 2. For martensitic PTs, the actual (optimal) orientation is determined from the minimum of the Gibbs energy or (when the external stresses are lacking) from the minimum of the energy of internal stresses g^e.[19] During nucleation, the mutual orientations with higher energy may also appear but because they have higher elastic and activation energy, they are less probable. For our more complex transformation process $1 \to 2_{stressed} \to$ virtual melt $\to 2_{relaxed}$, the situation may be opposite. The stressed phase 2 represents an activated state and if elastic energy g^e for optimal orientation of the crystal lattices is not sufficient to cause the virtual melting, it will transform back to the phase 1. At the same time, a nonoptimal orientation of the stressed phase 2, leading to higher g^e and having lower probability to appear, increases the probability of virtual melting and, consequently, completing the $1 \to 2_{stressed} \to$ virtual melt $\to 2_{relaxed}$ PT process.

Let us consider the more general case when the change in surface energy in eq 3 during the nucleation of the stressed coherent phase 2 is positive but small (for a large change in surface energy, nucleation requires high activation energy and is improbable) (Figure 2b). In this case, the critical nucleus of the stressed phase 2 will have the shape of a thin penny-shaped ellipsoid and parameters determined in refs 2 and 3, that is, the above evaluation of the internal stresses and elastic energy is still valid. If its energy is equal (or slightly smaller) than the melt Gibbs energy g_m, the virtual melting will occur as the thermodynamic (i.e., $f_{2\to m} = 0$) or thermally activated (for $f_{2\to m} < 0$) process. In both cases, according to Figure 2, eq 13 in eq 14 is valid again.

Let consider the next case, when a thermally activated subcritical nucleus of the stressed phase 2 appears, which without virtual melting has to transform back. However, if the existence time of this subcritical nucleus is sufficient for virtual melt nucleation, as the thermodynamic (i.e., $f_{2\to m} = 0$) or thermally activated (for $f_{2\to m} < 0$) process, then the transformation process $1 \to 2_{stressed} \to$ virtual melt $\to 2_{relaxed}$ will be completed. Thus, the virtual melting causes in some cases stabilization of the subcritical nucleus.

Note that in some cases the virtual melting can start during the growth of the transformation strain from zero to the value when the melting criterion is satisfied, that is, before completing the $1 \to 2_{stressed}$ PT.

4. Experimental Validation for the $\beta \leftrightarrow \delta$ Phase Transformations in the HMX Energetic Crystal

The organic nitramine ocathydro-1,3,5,7-tetranitro-1,3,5,7-tetrazocine $[CH_2-N(NO_2)]_4$ (HMX) is widely used in explosives. The main HMX phases of interest here are[10,11,13,20,21] (a) a monoclinic β phase which is stable at $\theta < 382.4$ K, (b) an orthorhombic α phase which is stable in the temperature range of $382.4 < \theta < 435$ K, (c) a hexagonal δ phase which is stable at $\theta > 435$ K, and (d) a γ phase which stability region is not exactly known but it is presumably between the α and δ phases; it may be also a metastable phase.

The melting temperature of the δ phase is 551 K and is 520 K for the β phase.

Equilibrium phase diagram at normal pressure is presented in Figure 3a. Parts b and c of Figure 3 represent the PT diagrams where all actually occurring PTs are shown, as well as all PTs which are expected but were not observed. The "normal" (expected) behavior is observed for $\alpha \to \delta$ PT which starts with significant overheating (at 461 K,[20,21] while the phase equilibrium temperature is 435 K). This overheating can be traditionally explained by the nucleation barrier, elastic energy, and athermal interface friction. The absence of the $\beta \leftrightarrow \alpha$ and $\delta \to \alpha$ PTs (above 400 K)[10,11,13,21] can be explained by the same reasons and demonstrates that these barriers are high. It is, however, completely unusual that the $\beta \leftrightarrow \delta$ PTs start practically without temperature hysteresis near the $\beta-\delta$ phase equilibrium temperature of 432 K.[10,11] This is despite the two times larger volumetric strain than for all other PTs in this system, which implies a two times larger athermal friction k and four times larger elastic energy g_e. We will analyze in this section these PTs in detail and will show that the only possible explanation is that the $\beta \leftrightarrow \delta$ PTs occur via virtual melting, while for other PTs, volumetric strain is not large enough to cause the melting. The importance of volumetric strain for this system also follows from the occurrence at room temperature of the $\delta \to \alpha$ PT, instead of (or along with) the $\delta \to \beta$ PT.[11,21]

It has long been suspected that chemical decomposition may play a role in the PT; see for example ref 27. And it is possible that decomposition plays a role when rates of heating are such

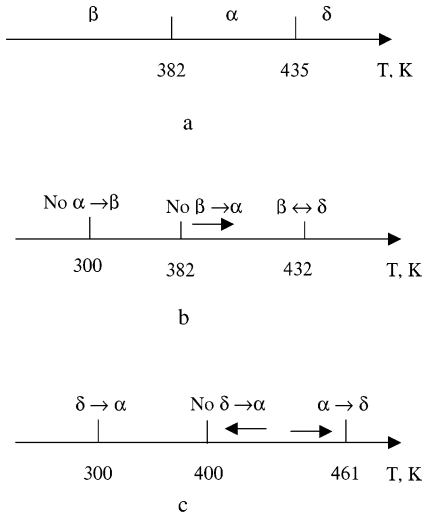

Figure 3. Puzzles of HMX polymorphism that can be resolved by the virtual melting mechanism: (a) equilibrium phase diagram; (b) $\beta \leftrightarrow \delta$ PTs occur near the phase equilibrium temperature (which is unusual for solid−solid PTs with large volumetric strain); $\beta \rightarrow \alpha$ PT is not observed despite the two times smaller volumetric strain than that for the $\beta \rightarrow \delta$ PT; the $\alpha \rightarrow \beta$ PT also was not observed at room temperature (in the region of stability of the β phase); (c) the $\alpha \rightarrow \delta$ PT starts with significant overheating despite the two times smaller volumetric strain than that for $\beta \rightarrow \delta$ PT; the $\delta \rightarrow \alpha$ PT has not been observed above 400 K (in the region of stability of the α phase) but occurs at room temperature (in the region of stability of the β phase). Only $\beta \leftrightarrow \delta$ PTs occur via the virtual melting which removes the temperature hysteresis. Volumetric strain for other PTs is not sufficient for melting which explains the large temperature hysteresis due to elastic stresses and interface friction.

that the PT is delayed to temperatures above 458 K. However, in our experimental studies[10,11] which are used to justify the virtual melting, it was clearly shown that decomposition was negligible and that no time-dependent process other than those related to the $\beta-\delta$ PT was influencing the mechanism of transformation. Specifically, the experiments in refs 10 and 11 were carried out at temperatures below 448 K such that no significant decomposition was observed in the samples studied. This assessment was based on optical microscopy and Raman spectroscopy and therefore indicated a fractional sensitivity of a few percent. More importantly, the transition was driven in the forward $\beta \rightarrow \delta$ direction and in reverse from the δ to β phase. The transformation was also cycled several times for the same sample with the kinetics being invariant and reproducible each time. We conclude that a significant effect due to decomposition would constitute a time-dependent perturbation to the PT process, and we did not observe it.

In this section, we will use the available experimental data to confirm the mechanism of $\beta \leftrightarrow \delta$ PTs via virtual melting. A typical experiment that we used for our analysis consists of heating and cooling of the sample according to a chosen program with no external forces and with the measurement of the kinetics (in terms of volume fraction or interface velocity) for the chosen PT. For example, in refs 10 and 11, the sample was heated to the various prescribed temperatures and held at constant temperature until the $\beta \rightarrow \delta$ PT was complete followed by a reduction of temperature below θ_e and holding at constant temperature until the $\delta \rightarrow \beta$ PT was complete. For some experiments, two cycles of direct-reverse PTs have been performed. The damage after the PT was evaluated visually.

(a) Thermodynamic Possibility of Virtual Melting during the $\beta \rightarrow \delta$ PT. Let us estimate whether virtual melting can occur at the $\beta-\delta$ phase equilibrium temperature 432 K, which is 119 K lower than the melting temperature of δ phase $\theta_m = 551$ K. By extrapolating data from ref 22 for $\theta = 432$ K for the δ phase and for the melt, we obtain $\Delta s_{\delta\rightarrow m} = 132.70$ J/(mol K), $\Delta h_{\delta\rightarrow m} = 66272.3$ J/mol. Substituting these data in eq 5, one obtains that the elastic energy g^e necessary to melt the stressed δ phase is $g^e = 8.947$ kJ/mol. (In ref 14, for 430 K, we obtained $\Delta s_{\delta\rightarrow m} = 132.83$ J/(mol K), $\Delta h_{\delta\rightarrow m} = 66188.3$ J/mol, and the elastic energy g^e necessary to melt the stressed δ phase was $g^e = 9.072$ kJ/mol.) We will use the molecular weight $M \simeq 0.296$ kg/mol and the mass density $\rho = 1650$ kg/m^3,[23] such that $V_m = M/\rho = 1.8 \times 10^{-4}$ m^3/mol. The elastic properties of the β and δ phases are pressure dependent and very uncertain.[23,24] Note that the transformed layer of the δ phase is under significant internal pressure (see below). We will take some intermediate values for the bulk modulus $B = 15$ GPa and the shear modulus $\mu = 7$ GPa; the Poisson ratio is then $\nu = (3B - 2\mu)/2/(3B + \mu) = 0.298$. The actual mechanism of transformation of the monoclinic β phase into the hexagonal δ phase is unknown, and the only known volumetric transformation strain is $\epsilon_0 \simeq 0.08$.[23] We assume $\epsilon^t_{11} = \epsilon^t_{22} = 1/2\epsilon^t_{21}$ and find the value ϵ^t_{11} required for melting from the condition $g^e = 8.947$ kJ/mol. The value obtained $\epsilon^t_{11} = 0.0247$ is reasonable because it is smaller than $\epsilon_0/3 = 0.027$. For $\theta_e = 430$ K, we obtained $\epsilon^t_{11} = 0.025$.[14]

Note that, at $\theta_m = 551$ K, the experimental value $\Delta h_{\delta\rightarrow m} = 69.9 \pm 4.2$ kJ/mol.[22] Calculations in refs 10 and 25 and here are based on $\Delta h_{\delta\rightarrow m} = 69.9$ kJ/mol. The indeterminacy in the enthalpy change is approximately half of the required elastic energy. If we take the lower bound for $\Delta h_{\delta\rightarrow m}$ and subtract 4.2 kJ/mol from the required elastic energy, then we obtain $\epsilon^t_{11} = 0.018$.

If the elastic energy $g^e < 8.947$ kJ/mol for optimal mutual orientation between the crystal lattices of the β and δ phases (which is currently unknown), then a nonoptimal orientation will be chosen by the system to complete the transformation process $\beta \rightarrow \delta_{stressed} \rightarrow$ virtual melt $\rightarrow \delta_{relaxed}$ (as was discussed in section 3). All other cases considered at the end of Section 3 (when elastic energy g^e is not sufficient for the melting, when change in surface energy creates an additional barrier, and when virtual melting stabilizes a subcritical nucleus) are applied to $\beta \rightarrow \delta$ PT as well.

We conclude that the elastic energy can be responsible for the significant reduction in melting temperature and that the suggested mechanism of stress relaxation and loss of interface coherence via intermediate melting is quite plausible.

Note that the local stresses, eq 6, are much higher than the macroscopic yield stress at compression $\sigma_y = 0.26$ GPa.[23] For $\epsilon^t_{11} = \epsilon^t_{22} = 1/2\epsilon^t_{22} = 0.025$, $\sigma_{11} = \sigma_{22} = 0.322$ GPa, however, $\sigma_{12} = 0.695$ GPa which is much greater than the yield stress in shear $\tau_y = 1/2\sigma_y = 0.13$ GPa. However, because the stresses are localized in a very thin layer, the probability of the existence of dislocations and dislocation sources is negligible, and local yield stress may approach the theoretical strength of the crystal. Stress states much higher than the yield stresses are well-known for other crystalline materials, for example, for the case of precipitates and nuclei.[2]

(b) Overall Kinetics of the $\beta \rightarrow \delta$ PT. Equation 16 for the rate of volume fraction coincides with eq 13 in ref 10 for the growth stage. Our activation energies, $E_{1\rightarrow2} = \Delta g_{1\rightarrow m}$ and $E_{2\rightarrow1} = \Delta g_{2\rightarrow m}$, are equal to the melting energy of phases 1 and 2, respectively. They coincide with activation energies postulated and experimentally confirmed in ref 10. The temperature dependence of the rate constant is determined by the heat of fusion, $h_{2\rightarrow m}$, like in experiments and in eq 13 in ref 10. Figure

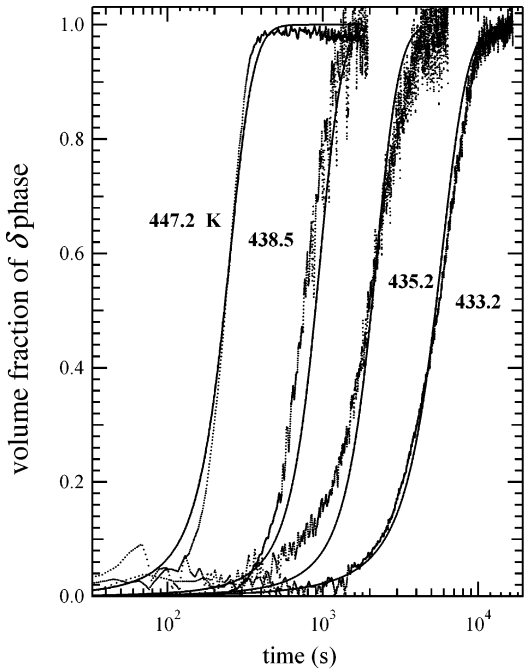

Figure 4. Comparison of the predictions based on the virtual melting mechanism for kinetic curves $c(t)$ (solid line[26]) with experimental data for the $\beta \rightarrow \delta$ PT in the HMX-based plastic bonded explosive PBX 9501[10,11] under isothermal conditions. The volume fraction of the δ phase c is equal to the square root of the measured second harmonic generation intensity from the HMX δ phase.

4[26] shows a good correspondence between the predictions based on the virtual melting mechanism and experiments from refs 10 and 11.

(c) Interface Velocity. In our experiments, an optical movie of the $\beta-\delta$ interface motion in a single HMX crystal (without binder) was recorded under isothermal conditions at three temperatures: 443, 450, and 458 K. The interface velocity v at several PT stages was determined by dividing the small normal interface displacement by the corresponding propagation time (see diamonds in Figure 5). The reported average of similarly obtained measurements from ref 12 are shown as squares in Figure 5. The data shown as triangles in Figure 5 are obtained from the equation $v = l/t_{0.5}$, where $t_{0.5}$ is the half transformation time reported in ref 11 (determined by second harmonic generation experiments) and l is the effective propagation length (the same for all points and chosen to yield best fit). A change in l shifts all triangles in the vertical direction by the same value. The data shown as circles in Figure 5 are experimental data reported in ref 12 obtained using the width of the differential scanning calorimetry (DSC) endotherms of individual particles (to determine the full transformation time), the particle mass and density (to determine the particle volume), and an assumption that the propagation path is 1.5 of the effective spherical diameter of the particle. Our calculations (curves 1 in Figure 5) were based on eq 14 with $\Delta h_{\delta\rightarrow m} = 69.9$ kJ/mol and $-\Delta g_{1\rightarrow 2} = \Delta s_{1\rightarrow 2}(\theta - \theta_e)$, where $\theta_e = 432$ K,[13] $\Delta h_{1\rightarrow 2} = 9.8$ kJ/mol, and $\Delta s_{1\rightarrow 2} = \Delta h_{1\rightarrow 2}/\theta_e = 22.68$ J/(mol K). Thus, the final expression for the $\beta-\delta$ interface velocity in our theory is

$$v = \bar{v}_0 \exp(-8407/\theta)\left(\exp\left(\frac{2.7279(432-\theta)}{\theta}\right) - 1\right) (\mu\text{m/s}) \quad (17)$$

where the two first multipliers are combined in $\bar{v}_0$. Our middle curve 1 in Figure 5 is plotted for $\bar{v}_0 = 10^{10}$ μm/s. A change in the preexponential multiplier by a factor of 2.1 shifts the middle curve up and down by 0.32. Note that, if we normalize all points in Figure 5 with the interface velocity at any temperature, the preexponential factor cancels. Thus, good correspondence between temperature dependence of the interface velocity in the experiment and our theory is independent of the fitting parameter $\bar{v}_0$. Line 2 in Figure 5 represents a fit suggested in ref 12 for their experimental data. For $1000/\theta < 2.19$, both approximations give very close results, while for $1000/\theta > 2.19$ (especially for $1000/\theta > 2.21$) the difference is drastic. The main difference is because of the choice of a different phase equilibrium temperature θ_e, which in turn changes the value of activation energy. The choice $\theta_e = 451$ K in ref 12 was probably motivated by thermodynamic data in ref 22, which gives such a θ_e; it is also consistent with the experiments in ref 27. The lowest PT temperature in HMX crystals (without a binder) is controlled by nucleation rather than a growth process. The binder (or more exactly, nitroplasticizer) provides an easier mechanism for nucleation,[28] reducing the PT start temperature to something closer to the equilibrium temperature. Namely, the HMX β phase dissolves in the nitroplasticizer and nucleates in the form of the δ phase at the interface between the HMX and binder, above θ_e. The binder does not affect the interface propagation which occurs inside the HMX crystal. Since in our experiments[10,11] the PT in HMX with a binder was observed at a lower temperature of 432.6 K, then the phase equilibrium temperature $\theta_e \leq 432.6$ K. The phase equilibrium temperature may depend on impurities (in particular, RDX). According to ref 13, the lowest temperature when $\beta \rightarrow \delta$ PT is observed in a solution is 432 K which we use as θ_e in this paper. Also, $\theta_e = 432$ K provides the best fit for the interface velocity experiments in Figure 5. Note that in ref 29 $\theta_e = 431$ K.

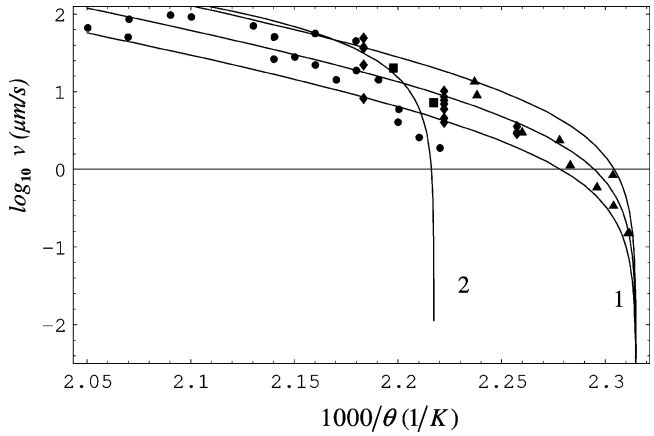

Figure 5. Comparison of the predictions for the temperature dependence of the interface velocity with experiments. The data are plotted as the logarithm of the interface velocity (log v) as a function of the inverse temperature ($1000/\theta$). Data based on our direct measurements of the propagation of the interface using optical movies of the visible opacity change are plotted as diamonds; data from similar measurements from ref 12 are plotted as squares; data obtained from the equation $v = l/t_{0.5}$, where $t_{0.5}$ is the half transformation time from refs 10 and 11 and l is the effective propagation length (chosen from the best fit), are plotted as triangles; experimental data from ref 12 obtained using DSC measurements are plotted as circles. Lines 1 are based on our eq 17 with three different preexponential factors, $\bar{v}_0 = 10^{10}$ μm/s for the middle curve; a change in the preexponential factor shifts the middle curve up and down by 0.32. Line 2 is a fit suggested in ref 12.

Our eq 17 describes well all experimental data from ref 12 except three points for $1000/\theta = 2.20-2.22$ (Figure 5). The lower v values for these experiments can be attributed to the error in the propagation length in DSC tests, because direct measurements of v in ref 12 (squares in Figure 5) give much higher values; these points will not be taken into account. Then,

a good description of all (ref 12 and this paper) the experiments on interface propagation by our equation based on the virtual melting theory can be considered as one more piece of evidence regarding the validity of the virtual melting hypothesis. The scatter in data can be described by the scatter in v_0 without changing the temperature dependence.

(d) Absence of the $\beta \rightarrow \alpha$ PT. Note that, in the temperature range $382.4 < \theta < 435$, the orthorhombic α phase is stable, that is, $\beta \rightarrow \alpha$ PT is expected to occur but does not.[10,11] Because the volumetric transformation strain for $\beta \rightarrow \alpha$ PT is two times smaller than that for the $\beta \rightarrow \delta$ PT, that is, $\epsilon_0^{\beta\rightarrow\alpha} \simeq 0.5\epsilon_0^{\beta\rightarrow\delta}$, g^e is four times smaller, which (if the virtual melting were absent) should promote the $\beta \rightarrow \alpha$ PT in comparison with the $\beta \rightarrow \delta$ PT. As the threshold k is proportional to ϵ_0,[6,7] it should be two times smaller than that for the $\beta \rightarrow \delta$ PT.

On the other hand, since g^e and the resulting decrease in melting temperature for the $\beta \rightarrow \alpha$ PT is also four times smaller than that for the $\beta \rightarrow \delta$ PT, the virtual melting and stress relaxation cannot occur (in contrast to the $\beta \rightarrow \delta$ PT). Thus, virtual melting can explain the absence of the $\beta \rightarrow \alpha$ PT, which otherwise is contradictory.

The lack of a $\beta \rightarrow \alpha$ PT demonstrates that other stress relaxation mechanisms are not efficient or increase k, like plasticity and fracture usually do.[7] To estimate the driving force for the $\beta \rightarrow \alpha$ PT at $\theta = 432.6$, we will use the equation $-\Delta g_{\beta\rightarrow\alpha} = \Delta s_{\beta\rightarrow\alpha}(432.6 - \theta_{\beta-\alpha})$ with $\theta_{\beta-\alpha} = 382.4$ K and $\Delta s_{\beta\rightarrow\alpha} = 28.8$ J/(mol K).[20,29] This leads to the value $-\Delta g_{\beta\rightarrow\alpha} = 1.446$ kJ/mol characterizing $k + g^e$ for the $\beta \rightarrow \alpha$ PT under actual mechanisms of stress relaxation.

Note that the $\beta \rightarrow \gamma$ and $\alpha \rightarrow \gamma$ PTs, which have a small transformation strain in comparison with the $\beta \rightarrow \delta$ PT, should also occur prior the $\beta \rightarrow \delta$ and $\alpha \rightarrow \delta$ PTs but they do not. However, because the region of stability of the γ phase, as well as the driving force for the above PTs, are unknown, these results cannot be currently used as a valuable support of the virtual melting mechanism.

(e) Absence of Elastic Energy and Athermal Resistance to the Interface Motion for the $\beta \rightarrow \delta$ PT. In our experiments,[10,11] the $\beta \rightarrow \delta$ PT begins at 432.6 K, that is, immediately above the equilibrium temperature $\theta^e = 432$;[13] that implies that $k \simeq g^e \simeq 0$, which is very unusual for a solid−solid PT with large ϵ_0. This is possible for a PT through a liquid phase only, because other relaxation mechanisms (dislocation and crack generation) increase k. As an example, for martensitic unit growth in a steel, finite element calculations show that the value K increases from 2.35 to 30 MPa due to plastic flow.[30] We estimate the transition temperature in the absence of virtual melting by taking $k + g^e = 1.446$ kJ/mol (like for the $\beta \rightarrow \alpha$ PT). Then the lower bound for $\theta^e_{\beta\rightarrow\delta} = (9.8 + 1.446)/0.02268 = 495.85$ K instead of $\theta_{\beta\rightarrow\delta} = 432.6$ K. It is clear that without stress relaxation via virtual melting, the $\beta \rightarrow \delta$ PT could not occur by propagation of the coherent interface. Furthermore, the only possible mechanism for propagation of the incoherent interface would be atom by atom.

(f) Nanocracking. Considerable cracking (voiding), homogeneously distributed in the transformed material over the several hundred nanometer scale accompanies the PT,[11] see Figure 6, as predicted by theory. It is detected by a strong increase in visible light scattering. Transparent, pristine β-phase HMX crystals, approximately 500 μm long (Figure 6a), transform to opaque δ-phase crystals (Figure 6b). The opaqueness is caused by voids or cracks distributed at the scale of hundreds nanometers. Atomic force microscopy[31] demonstrates directly the generation of the voids during the $\beta \rightarrow \delta$ PT that finishes upon completion of the PT.

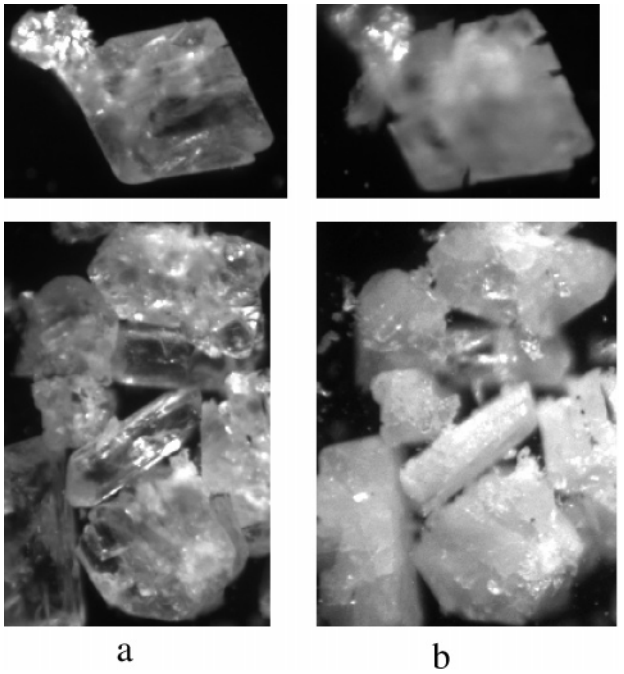

Figure 6. Transparent β phase HMX crystals (a) and opaque δ phase crystals (b) after the $\beta \rightarrow \delta$ PT. The opaqueness is caused by cracks distributed at the length scale of hundreds of nanometers. Without virtual melting, only macroscopic cracks would be expected.

Without virtual melting, stresses during the $\beta \rightarrow \delta$ PT in the V_n are compressive, because transformation volumetric strain is tensile. Compressive stresses cannot cause nanocracking. Also, in the solid phase, cracks initiate heterogeneously at local stress concentrators (dislocations, grain, subgrain, and twin boundaries) and propagate to the more macroscopic size. It is hard to imagine that the spacing between stress concentrators is so small. This experimental evidence strongly supports the virtual melting mechanism.

According to ref 10 (Table 2), the volumetric strain due to solidification of the δ phase $\epsilon_0^{s,\delta} = -1.19\epsilon_0^t/1.14 = -0.0835$. The volumetric strain due to nanocracking (see section 2), $\epsilon_0^c = -2\epsilon_0^s/3 = 0.0557$, which is the upper bound for the porosity induced by this mechanism during the $\beta \rightarrow \delta$ PT.

On the scale of the whole crystal, one more type of internal stresses (microscale rather than nanoscale) is generated. Assume for simplicity that the δ phase has the spherical shape inside the spherical matrix of the β phase. The corresponding solution of the elastic and elastoplastic problem can be found, for example, in ref 32. The solutions indicate that, independent of the condition at the interface (coherent or incoherent) in the elastic regime, the volumetric transformation strain and strain due to nanocracking induce compressive pressure in the inclusion, $p = (\epsilon_0^t + \epsilon_0^s)/C$, where $C = 9(1 - \nu)/(2E) = 0.175$ GPa^{-1}, that is, $p = 0.775$ GPa. This pressure significantly exceeds the macroscopic yield strength $\sigma_y = 0.26$ GPa.[23] Such a high pressure will close nanocracks (pores) in the transformed δ phase. Thus, internal nanocrack interfaces (which cause observable light scattering) remain but not nanocrack volumes. This reduces the pressure in the δ phase inclusion to $p = \epsilon_0^t/C = 0.457$ GPa. Still, this pressure exceeds essentially the limit pressure $p_y = 2/3\sigma_y = 0.173$ GPa, which can be carried by the infinite matrix elastically.[32] The overstresses can relax through plastic straining (according to solution in ref 32). Alternatively, the tensile hoop stress in the matrix, if it exceeds the fracture

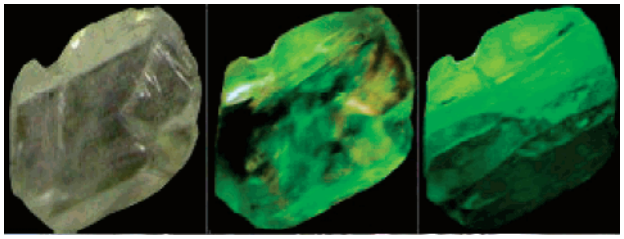

Figure 7. $\beta \rightarrow \delta$ PT images via second harmonic generation. White corresponds to the β phase and green to δ phase.

limit, will cause damage and macrocracking. Macroscopic cracks in Figure 6b are caused by these tensile stresses. Without virtual melting, only macroscopic cracks would be expected. Thus, the macrocracks observed in Figure 6b are consistent with virtual melting.

If HMX crystals are elongated in one direction, then after the δ phase reaches the free lateral surfaces (see Figure 4 and the movie in ref 12), the solution for sphere is not applicable even approximately. If the interface is planar, then in the presence of virtual melting, internal stresses in the remaining β phase are absent. Without virtual melting, tensile stresses in the β phase and macrocracks will be present even for the plane interface. This may serve as an additional signature for virtual melting. Also, opaqueness of the δ phase only and transparency of the remaining β phase would serve as an additional argument supporting virtual melting. For elongated samples, volume increase due to nanocracking will not be compensated by compressive pressure, like in the case of an inclusion in the matrix. Since experiments were conducted before the appearance of the virtual melting hypothesis, we did not pay proper attention to these details and cannot strictly confirm them. On the other hand, the remaining β phase in Figure 7 looks transparent. Also, macrocracks are observed in Figure 6b in the sample which has approximately equisized shape, for which the previous approximation by spherical inclusion inside the spherical matrix is a good one. For elongated samples (see Figure 4 and movie in ref 12), macrocracks are not observed which corresponds to the case with virtual melting (see above). The total volume expansion during the $\beta \rightarrow \delta$ PT was measured in ref 33 to be 0.15−0.17. Since $\epsilon_0 = 0.08$ and nanocracking after solidification results in $\epsilon^c = 0.056$, it is reasonable that the resulting macrocracks are related to the relatively small expansion of 0.014−0.034.

Note that the nanocracking of the δ phase, induced by the $\beta \rightarrow \delta$ PT, can be a reason for the higher sensitivity of the δ phase. It may create hot spots by the nanovoid collapse mechanism or by the friction at nanocrack surfaces.

(g) Independence of the Thermodynamics and Kinetics of the $\beta \rightarrow \delta$ PT of Nanocracking. It is expected that any irreversible process (fracture or plasticity), which accompanies the PT, would significantly affect its thermodynamics and kinetics; see as examples refs 8, 30, and 34. Our theory based on the virtual melting mechanism predicts the opposite, namely, that nanocracking should not affect the thermodynamics and kinetics of the $\beta \rightarrow \delta$ PT. Indeed, in our experiments,[11] the nanocracking did not change the PT thermodynamics and kinetics appreciably. In particular, the PT started just above the equilibrium PT temperature and it is well described by kinetic eq 16 without any contribution from the nanocracking to activation energy and thermodynamic driving force for the PT.

(h) Overheating for the $\alpha \rightarrow \delta$ PT. The $\alpha \rightarrow \delta$ PT starts at the temperature of 461 K[20,21] which is significantly higher than the $\alpha-\delta$ phase equilibrium temperature of 435 K given in ref 13. This can easily be explained by the absence of virtual melting, because the volumetric transformation strain for the $\alpha \rightarrow \delta$ PT, $\epsilon_0^{\alpha\rightarrow\delta} = 0.046$[21] and is therefore too small to cause virtual melting. Note that the virtual melt could also be crystallized into the stable α phase below 435 K along the transformation path $\beta \rightarrow \delta_{\text{stressed}} \rightarrow$ virtual melt $\rightarrow \alpha_{\text{relaxed}}$. However, after virtual melting of the stressed δ phase, the melt has a short-range order structure corresponding to the δ phase and solidification can be faster to the δ phase rather than the α phase. Alternatively, the $\alpha-\delta$ phase equilibrium temperature may be below 432.6 K, for example, 430 K. To estimate the driving force for the $\alpha \rightarrow \delta$ PT at 461 K, which is equal to $k + g^e$, we use $-\Delta g_{\alpha\rightarrow\delta} = \Delta h_{\alpha\rightarrow\delta}(461-435)/435 = 0.400$ kJ/mol, where $\Delta h_{\alpha\rightarrow\delta} = 6.7$ kJ/mol was taken from ref 21.

Note that the $\gamma \rightarrow \delta$ PT starts at 444 K and is accompanied by a small volumetric transformation contraction of −0.033.[20,21] This PT cannot occur via virtual melting, and if we knew that the $\gamma \rightarrow \delta$ phase equilibrium temperature was significantly lower than 444 K, then it would be one more piece of evidence supporting the virtual melting mechanism for the $\beta \rightarrow \delta$ PT. However, there are currently no data in the literature on the $\gamma \rightarrow \delta$ phase equilibrium temperature.

(i) Thermodynamic Possibility of Virtual Melting during the Reverse $\delta \rightarrow \beta$ PT. Let us estimate whether virtual melting can occur during the reverse $\delta \rightarrow \beta$ PT, and if yes, then above which temperature. We consider the following transformation process $\delta \rightarrow \beta_{\text{stressed}} \rightarrow$ virtual melt $\rightarrow \beta_{\text{relaxed}}$, and we need to estimate whether melting of the stressed β phase can occur below 432 K. For the reverse $\delta \rightarrow \beta$ PT, the transformation strain tensor $\epsilon^t_{\delta\rightarrow\beta} = -\epsilon^t_{\beta\rightarrow\delta}$ in the transformed layer causes tensile stresses of the same magnitude as the compressive stresses during the $\beta \rightarrow \delta$ PT. As it follows from eq 7, the elastic energy of internal stresses g^e is the same for the direct $\beta \rightarrow \delta$ PT and the reverse $\delta \rightarrow \beta$ PT and will be taken as $g^e = 8.947$ kJ/mol. We will show now that such an elastic energy can cause the virtual melting of the β phase down to the temperatures 400−412 K.

Taking data from ref 22 for the β phase at $\theta = 400$ K ($h_\beta = 78.767$ kJ/mol and $s_\beta = 387.543$ J/(mol K)) and extrapolating data from ref 22 for the melt to 400 K ($h_m = 152.743$ kJ/mol and $s_m = 544.786$ J/(mol K)), we obtain from eq 5 that the melting temperature of the stressed β phase is $\theta^e_m = 413.6$ K. However, if for the case without internal stresses ($g^e = 0$) we substitute in eq 5 interpolated (for the β phase) and extrapolated (for the melt) data from ref 22 at $\theta = 520$ K (the melting temperature of the β phase[13]), then we obtain $\theta_m = 531.3$ K instead of 520 K. The data from ref 22 therefore overestimate the melting temperature by ∼10 K, and if we take that into account, then we may conclude that the virtual melting of the stressed β phase can occur above 400−414 K. Indeed, there is a small jump in the kinetic data (see Figure 7 in ref 11) between the two experiments at 417 and 394 K, which may serve as an indication of the change in growth mechanism. It is not clear, however, why the change in the mechanism leads to the slight increase in rate rather than to a decrease. We may speculate that, below 400 K, the $\delta \rightarrow \alpha$ PT first (or also) occurs because it has two times smaller volumetric transformation strain and four times smaller elastic energy. Note that the second harmonic generation method does not allow distinction between the δ and α phases; FTIR did not identify the α phase[11] which still does not exclude the presence of a small amount. Tensile stresses generated by the α phase increase the driving force for the $\delta \rightarrow \beta$ PT. Alternatively, some β crystals may nucleate and grow via virtual melting during cooling in the temperature range 400−

430 K. They can facilitate the $\delta \rightarrow \beta$ PT below 400 K due to the well-known autocatalytic effect.[4,20]

Note that, if high temperature is reached during or after the $\beta \rightarrow \delta$ PT, chemical decomposition may occur. This may reduce the melting temperature and may broaden the temperature interval in which the virtual melting occurs during the $\delta \rightarrow \beta$ PT.

Below 400 K, traditional mechanisms of stress relaxation at the moving interface, probably through cracking, have to occur. If damage as a relaxation mechanism is suppressed, then the diffusive atom by atom PT will occur. Since the temperature is low, it can be quite slow, as observed in experiments.[10−12]

(j) Overall Kinetics of the $\delta \rightarrow \beta$ PT. Equation 16 for the rate of volume fraction can be used for the reverse PT for the driving force $-\Delta g_{1\rightarrow 2} < 0$. It coincides with eq 13 in ref 10 for the growth stage which is also used for both direct and reverse PTs. Our activation energies, $E_{1\rightarrow 2} = \Delta g_{1\rightarrow m}$ and $E_{2\rightarrow 1} = \Delta g_{2\rightarrow m}$, coincide with activation energies postulated and experimentally confirmed in ref 10. The temperature dependence of the rate constant is determined by the heat of fusion $h_{2\rightarrow m}$, like in experiments and in eq 13 in ref 10. Note that eq 16 for the $\delta \rightarrow \beta$ PT can be used above 400−412 K only. At lower temperatures, virtual melting cannot occur and an alternative kinetic equation has to be developed.

(k) Absence of the $\delta \rightarrow \alpha$ PT above 400 K. Note that in the temperature range $382.4 < \theta < 435$ K, the orthorhombic α phase is stable, that is, a $\delta \rightarrow \alpha$ PT rather than a $\delta \rightarrow \beta$ PT should occur. Since the volumetric transformation strain for the $\delta \rightarrow \alpha$ PT is two times smaller than that for the $\delta \rightarrow \beta$ PT, g^e and k are four and two times smaller, respectively, which have to favor the $\delta \rightarrow \alpha$ PT. However, the $\delta \rightarrow \beta$ PT only was observed in the temperature range $430 > \theta > 400$ K.[10,11] This can be explained by the virtual melting of the β phase while the virtual melting of the α phase is impossible, because its elastic energy and decrease in melting temperature is four times smaller. To estimate the driving force for the $\delta \rightarrow \alpha$ PT at 394 K (at this temperature, the $\delta \rightarrow \alpha$ PT still has not been observed in refs 10 and 11), which is equal to $k + g^e$, we use $-\Delta g_{\delta\rightarrow\alpha} = \Delta h_{\delta\rightarrow\alpha}(394-435)/435 = 0.631$ kJ/mol, where $\Delta h_{\delta\rightarrow\alpha} = -6.7$ kJ/mol.[21] This value has the same order of magnitude as 0.400 kJ/mol for the $\alpha \rightarrow \delta$ PT. A slightly higher value may be related to the lower by a 71 K temperature.

(l) Occurrence of the $\delta \rightarrow \alpha$ PT at Room Temperature in the Region of Stability of the β Phase. In our experiments, cooling the δ phase down to room temperature and keeping it over several days lead to the appearance of the α phase along with the β phase. This happens despite the fact that it is a much lower temperature than the $\beta \rightarrow \alpha$ phase equilibrium temperature of 382.4 K, that is, it is deeply in the region of stability of the β phase. Thus, the $\delta \rightarrow \alpha$ PT does not occur in the region of stability of the α phase (see item k) but occurs in the region of stability of the β phase, which sounds very paradoxical. However, since the virtual melting cannot occur at room temperature, elastic energy and interface friction contribute significantly to the thermodynamic barrier for the PT. The volumetric transformation strain for the $\delta \rightarrow \alpha$ PT is two times smaller than that for the $\delta \rightarrow \beta$ PT and g^e and k are four and two times smaller, respectively. This difference makes the net driving force $F_{1\rightarrow 2}$ for the $\delta \rightarrow \alpha$ at room temperature greater (or at least comparable) with that for the $\delta \rightarrow \beta$ PT.

The occurrence of the $\delta \rightarrow \alpha$ PT at room temperature was observed also in ref 21, where it was strongly dependent on the conditions of direct $\beta \rightarrow \delta$ and $\alpha \rightarrow \delta$ PTs (temperature and duration of holding at this temperature). In particular, for relatively high temperature (between 473 and 493 K) and holding time for the direct $\alpha \rightarrow \delta$ PT, the resulting δ phase transformed at room temperature to pure α phase, while at 463 K a mixture of α and β phases was observed at room temperature. Also, if the direct $\beta \rightarrow \delta$ PT occurs at 463 K for any holding time or at 473 or 483 K during short (0.5 h) time, then the resulting δ phase transformed at room temperature to pure β phase; for higher temperatures and a longer holding time, a mixture of α and β phases was observed at room temperature.

Such a history dependence can be hypothetically explained in the following way. When the $\beta \rightarrow \delta$ PT occurs at relatively low temperature or during short time, the PT is not complete and residual β phase is present. It grows during the reverse PT at room temperature and the α phase does not have time and proper nucleation sites to nucleate. At higher temperature and holding time for the $\beta \rightarrow \delta$ PT, the whole β phase transforms to the δ phase. During the reverse PT at room temperature, both the α and β phases have approximately equal probability to nucleate and grow due to comparable net driving force.

We may assume that the α phase does not completely transform to the δ phase at any temperature. When direct $\alpha \rightarrow \delta$ PT occurs at 463 K, this is not a conversion via the virtual melting mechanism and there are probably macroscopic regions of residual α phase. When this mixture is cooled to room temperature, significant stresses due to transformation strain and thermal stresses can nucleate the β phase at the interface between the α and δ phases. Then both the α and β phases grow simultaneously. At temperatures of 473 K and higher, the residual nuclei of the α phase which grow at room temperature are small. When such a system is cooled to room temperature, internal stresses are comparable with those for the case with 463 K but they act in a small region, perhaps smaller than the critical nucleus of the β phase. During the growth of the α phase, when the region of large internal stresses are large enough to nucleate the β phase, stress relaxation probably occurs via damage rather than through nucleation of the β phase. Also, relaxation of internal stresses during direct $\alpha \rightarrow \delta$ PT at 463 K can be different than at higher temperature and can result in differently damaged microstructure; this may contribute to the history-dependence of PTs at room temperature.

(m) Absence of the $\alpha \rightarrow \beta$ PT at Room Temperature.[10,11,21,13] The suppression of the $\alpha \rightarrow \beta$ PT cannot be explained by the high nucleation barrier, because both phases coexist simultaneously,[21] thus the sum $k + g^e$ is the only reason. To estimate the driving force for the $\alpha \rightarrow \beta$ PT at $\theta = 300$ K, we will use the equation $k + g^e = -\Delta g_{\alpha\rightarrow\beta} = \Delta s_{\alpha\rightarrow\beta}(300 - \theta_{\beta-\alpha}) = 2.373$ kJ/mol, where $\theta_{\beta-\alpha} = 382.4$ K and $\Delta s_{\alpha\rightarrow\beta} = -28.8$ J/(mol K).[20,29] The higher value in comparison with 1.446 kJ/mol for the $\beta \rightarrow \alpha$ PT (see item d) is expected because of the lower temperature.

(n) Small (negligible) Elastic Energy and Athermal Interface Friction for the $\delta \rightarrow \beta$ PT. In our experiments,[10,11] the $\delta \rightarrow \beta$ PT was observed very close to the $\delta-\beta$ phase equilibrium temperature (432 K) which we checked experimentally, namely, at 424 K. We believe that it would be observed at higher temperature as well. However, even such a small overcooling implies small $k + g^e \simeq 0.02266(432-424) = 0.181$ kJ/mol. This is negligible in comparison with the estimated value of $g^e = 8.947$ kJ/mol for this PT without virtual melting, as well as with values $k + g^e$ for all other PTs considered above. The only explanation which we see is that the $\delta \rightarrow \beta$ PT occurs via virtual melting.

(o) Nanocracking during the $\delta \rightarrow \beta$ PT. During virtual melting of the stressed β phase, all nano- and macrocracks,

crossed by the moving interface, disappear, deleting the entire thermomechanical prehistory. During solidification of the melt to the unstressed β phase, new nanocracking occurs. Since transformation strain during solidification of the β phase, $\epsilon_0^{s,\beta} = -(\epsilon_0^{s,\delta} + \epsilon_0^{\beta-\delta}) = -0.1635$, is two times greater than during solidification of the δ phase, the volumetric strain due to nanocracking $\epsilon_0^{c,\beta} = -2\epsilon_0^{s,\beta}/3 = 0.109$ is also two times greater. If the temperature is low enough and the $\delta \rightarrow \beta$ PT occurs without the virtual melting, then the same concentration of nanocracks (up to 0.0557) will be approximately kept but new macrocracks will appear due to the large volumetric transformation strain.

There are currently no experimental data to check this prediction of our theory, but they can be obtained in future. While the β phase obtained after PT reversal is indeed cracked, we do not have proof that these are new nanocracks after the virtual melting of the stressed β phase.

(p) Repeatability of the PT Kinetics during the Cyclic $\beta \leftrightarrow \delta$ PT. In our experiments on PBX 9501,[10,11] the kinetics of the second $\beta \leftrightarrow \delta$ cycle matched well the kinetics of the first $\beta \leftrightarrow \delta$ cycle. The temperatures for the direct and for the reverse PTs were 438 and 394 K, respectively. At the same time, experiments on HXM crystals in ref 12 exhibit differences in temperature range and in the transformation enthalphy for the first and second $\beta \rightarrow \delta$ PTs.

The main difference between the results in refs 10, 11, and 12 can easily be explained by the different nucleation mechanisms. The nucleation in the PBX 9501 formulation occurs at the boundary between HMX crystals and a nitroplasticizer.[28] Since the boundary provides numerous nucleation sites, the PT in HMX is growth-controlled rather than nucleation-controlled. Thus, some reduction in the total boundary area between HMX and a binder due to cracking during the first $\beta \leftrightarrow \delta$ cycle does not affect nucleation at the remaining boundary. On the other hand, in the HMX crystals without a binder,[12] nucleation occurs at the specific nucleating defects which may be inclusions of the solvent used in HMX synthesis[28] or some stress concentrators. Cracking and virtual melting during the first $\beta \leftrightarrow \delta$ cycle may destroy the nucleation sites and nucleation will occur at the less potent defects and will start at a higher temperature. In fact, the result in ref 12 that new cracks (stress concentrators) do not favor nucleation supports the hypothesis that nucleation in the HMX crystals without the binder is not related to stress concentrations and occurs via dissolution in the solvent inclusions. Since the nucleation during the second $\beta \rightarrow \delta$ PT starts at different places, the growth process will be different.

Another difference between the PT cycles in refs 10, 11, and 12 is that the reverse PT in refs 10 and 11 occurs at high temperature (394 K) and in ref 12 at low (mostly room) temperature. We do not expect virtual melting during the reverse PT at these temperatures. More cracks are expected in the sample in ref 12, because fracture toughness usually increases with the temperature. These cracks may arrest the growth, thus new nucleation is required to complete the PT. In refs 10 and 11, less and smaller macrocracks appear during the reverse $\delta \rightarrow \beta$ PT, and there is no problem with new nucleation if growth is arrested. Also, due to the binder, polycrystalline sample, and expansion during the $\beta \rightarrow \delta$ PT, the surfaces of cracks can be in contact and growth will not be arrested.

Now, let us compare two scenarios of the second $\beta \rightarrow \delta$ PT, when the $\beta \rightarrow \delta$ PT occurs without and with virtual melting. If there is no virtual melting, nanocracks (in fact, it is not clear how nanocracks distributed over the whole transforming volume appear without virtual melting) generated during the first $\beta \leftrightarrow \delta$ PT, as well as during the second $\beta \rightarrow \delta$ PT, affect the growth stage.[8] First, the stress field of the cracks creates an athermal resistance to interface propagation k, just as do other defects. Since the first $\beta \leftrightarrow \delta$ PT generates significant nanocracking, the magnitude of k for the second $\beta \rightarrow \delta$ PT would be much higher. It would shift the kinetic curve to higher temperatures. Second, new cracks will be generated during the second $\beta \rightarrow \delta$ PT, which will affect the thermodynamics and kinetics of the PT through changes in the stress field.[8]

If the first and second $\beta \rightarrow \delta$ PTs occur via virtual melting, then $k = 0$, and since the new nanocracks are generated during solidification (i.e., at negligible resistance to appearance of the crack), the stress field after the appearance of new nanocracks is zero, the same as before their appearance. This is similar to the first $\beta \rightarrow \delta$ PT. Thus, there is no reason the second $\beta \rightarrow \delta$ PT will differ from the first one, which corresponds to the experiment.[10,11]

Also, all cracks and other defects which appear during the first $\beta \rightarrow \delta$ PT disappear due to melting and new nanocracks appear during the solidification. Thus, there is no crack accumulation over the PT cycles; virtual melting deletes the entire thermomechanical memory of the previous $\beta \leftrightarrow \delta$ cycles. That is why the second reverse $\delta \rightarrow \beta$ PT does not differ from the first one, which also corresponds to the experiment.[10,11]

Thus, the repeatability of the PT kinetics during the cyclic $\beta \leftrightarrow \delta$ PT, observed experimentally in refs 10 and 11, is a very strong argument supporting the virtual melting mechanism of the $\beta \rightarrow \delta$ PT. Although the repeatability does not require virtual melting for the reverse $\delta \rightarrow \beta$ PT, when the reverse PT occurs via virtual melting (above 400 K), the same repeatability has to be observed.

5. Concluding Remarks

To summarize, there are 16 theoretical predictions which are in qualitative and quantitative agreements with experiments conducted on the $\beta \leftrightarrow \delta$ transformations in energetic crystal HMX. In particular:

(1) Decrease in the melting temperature due to internal stresses during the $\beta \rightarrow \delta$ PT, from 551 to 432 K.

(2) Decrease in the melting temperature due to internal stresses during the $\delta \rightarrow \beta$ PT, from 520 to 400 K; in both cases, the decrease in melting temperature is ~120 K.

(3) For the $\beta \rightarrow \delta$ PT, our activation energies, $E_{1\rightarrow 2} = \Delta g_{1\rightarrow m}$ and $E_{2\rightarrow 1} = \Delta g_{2\rightarrow m}$, are equal to the corresponding change in Gibbs potential for the melting. They coincide with activation energies postulated and experimentally confirmed in ref 10.

(4) For the $\beta \rightarrow \delta$ PT, the temperature dependence of the rate constant is determined by the heat of fusion $h_{2\rightarrow m}$, like in experiments and in eq 13 in ref 10. Our eq 16 for the rate of volume fraction coincides with eq 13 in ref 10 for the growth stage, which is confirmed experimentally (see Figure 4).

(5) The same results as in item 3 are valid for the reverse $\delta \rightarrow \beta$ PT.

(6) For the $\beta \rightarrow \delta$ PT, our eq 14 for the interface velocity correctly describes experimental data obtained in ref 12 and in this paper (Figure 5). Our activation energies for the direct and reverse PTs are equal to the corresponding change in Gibbs potential for melting, $E_{1\rightarrow 2} = \Delta g_{1\rightarrow m}$ and $E_{2\rightarrow 1} = \Delta g_{2\rightarrow m}$. The temperature dependence of the rate constant is determined by the heat of fusion $h_{2\rightarrow m}$.

(7) The $\beta \rightarrow \delta$ PT starts just above the $\beta - \delta$ phase equilibrium temperature, that is, elastic energy and athermal interface friction $k \simeq g^e \simeq 0$. This is in contrast to all known solid−solid transformations with a large volume change.

(8) The reverse $\delta \rightarrow \beta$ PT starts at very small driving force, that is, the elastic energy and athermal interface friction are negligible as well. If experiments were performed just below the $\beta-\delta$ phase equilibrium temperature, then maybe $k \simeq g^e \simeq 0$ would be obtained, like for the direct $\beta \rightarrow \delta$ PT.

(9) In contrast, the $\alpha \rightarrow \delta$ PT starts at a temperature higher by 31 K than the $\alpha-\delta$ phase equilibrium temperature. This corresponds to a quite high $k + g^e = 0.483$ kJ/mol. This can easily be explained by the absence of virtual melting, because the volumetric transformation strain for the $\alpha \rightarrow \delta$ PT is two times smaller and elastic energy as well as reduction in melting temperature are four times smaller than those for the $\beta \rightarrow \delta$ PT.

Note that the $\gamma \rightarrow \delta$ PT starts at 444 K and is accompanied by a small volumetric transformation contraction of -0.033.[20,21] This PT cannot occur via virtual melting, and if we knew that the $\gamma \rightarrow \delta$ phase equilibrium temperature is significantly lower than 444 K, then it would be one more piece of evidence supporting the virtual melting mechanism for the $\beta \rightarrow \delta$ PT.

(10) Considerable cracking, homogeneously distributed in the transformed material over the hundred nanometer length scale, accompanies the $\beta \rightarrow \delta$ PT, as predicted by theory. Without virtual melting, nanocracking would be impossible. Similar nanocracking is predicted for the reverse $\delta \rightarrow \beta$ PT and is also observed, but there are no clear data to separate it from the nanocracking during the direct PT.

(11) The nanocracking does not change appreciably the thermodynamics and kinetics for the $\beta \rightarrow \delta$ PT,[10,11] as predicted by theory. The virtual melting deletes the entire thermomechanical history.

(12) The thermodynamics and kinetics of the second $\beta \leftrightarrow \delta$ PT cycle do not differ appreciably from those of the first one,[10,11] as predicted by theory.

(13) The $\beta \rightarrow \alpha$ PT, which is thermodynamically possible in the temperature range $382.4 < \theta < 435$ K and has a two times smaller transformation strain than the $\beta \leftrightarrow \delta$ PT, does not occur. It cannot occur because the elastic energy is not sufficient to induce virtual melting. For a traditional mechanism of $\beta \rightarrow \alpha$ PT, the elastic energy and athermal resistance to the interface motion suppress the PT.

(14) The $\alpha \rightarrow \beta$ PT, which is thermodynamically possible below 382.4 K, was not observed at room temperature. The reason is the same as that in item 13.

(15) The $\delta \rightarrow \alpha$ PT, which is thermodynamically possible in the temperature range $382.4 < \theta < 435$ K and has a two times smaller transformation strain than the $\beta \leftrightarrow \delta$ PT, has not been observed above 400 K, while $\beta \leftrightarrow \delta$ PT does. The reason is the same as that in item 13.

(16) The $\delta \rightarrow \alpha$ PT occurs at room temperature in the region of stability of the β phase. This demonstrates the importance of the elastic energy and interface friction when virtual melting is impossible.

Note that the $\beta \rightarrow \gamma$ and $\alpha \rightarrow \gamma$ PTs, which also have a much smaller transformation strain than that for the $\beta \rightarrow \delta$ PT, should also occur prior to the $\beta \rightarrow \delta$ PT but they do not. However, because the region of stability of the γ phase, as well as the driving force for the above PTs, are unknown, these results cannot be currently used as a valuable support of the virtual melting.

The above confirmations are independent of each other. For example, any result for the $\beta \rightarrow \delta$ PT does not imply that a similar result has to be valid for the $\delta \rightarrow \beta$ PT. Good agreement for kinetics of single interface propagation does not imply good agreement for the overall kinetics, since the latter is also affected by nucleation and morphology of the growing regions. Independence of thermodynamics and kinetics of the $\beta \rightarrow \delta$ PT of the nanocracking does not imply that the same independence will take place for the first and second direct-reverse transformation cycles. Also, the absence of the $\beta \rightarrow \alpha$ PT in one temperature range does not imply the absence of $\alpha \rightarrow \beta$ or $\delta \rightarrow \alpha$ transformations in a different temperature range. We can however combine these confirmations in several groups. The results in items 1, 2, 7, and 8 are related to the thermodynamics of the $\beta \leftrightarrow \delta$ PTs. The results in items 3−6 are related to the kinetics of the $\beta \leftrightarrow \delta$ PTs. Items 10−12 describe interaction between PTs and the damage which cannot be explained without virtual melting. Finally, items 9 and 13−16 demonstrate that, for other PTs for which virtual melting is impossible, elastic energy and interface friction make significant contributions to the thermodynamics and kinetics which was not observed for the $\beta \leftrightarrow \delta$ PTs.

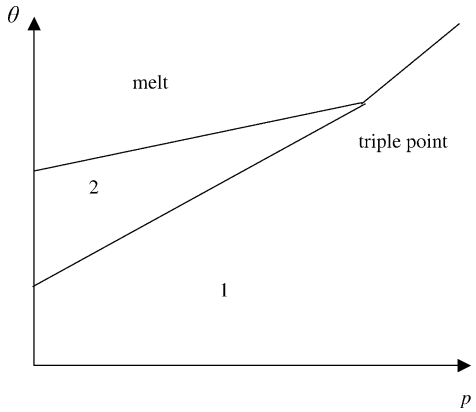

Figure 8. Pressure−temperature phase diagram which contains the triple (1−2−m) point. The increase in pressure makes θ_{1-2} and θ_{2-m} closer and increases the chance that virtual melting is the mechanism of solid−solid PT.

None of these results separately proves strictly the validity of the virtual melting mechanism. However, because it is difficult to imagine any other mechanism which explains all of the above 16 experimental results, we conclude that $\beta \leftrightarrow \delta$ PTs in the HMX crystal occur via virtual melting.

Thus, we have found a new mechanism of solid−solid PT, loss of interface coherence, and stress relaxation via virtual melting, far below the melting temperature. The mechanism significantly changes the thermodynamics (increases the net driving force $F_{1\leftrightarrow 2}$ up to $-g_{1\leftrightarrow 2}$ and eliminates the athermal interface friction k) and kinetics (activation energy and rate constant) of solid−solid PT and leads to nanocracking. Virtual melting deletes the entire thermomechanical memory about preceding $1 \leftrightarrow 2$ PT cycles. This mechanism can be operative for material systems, for which (a) the reduction in melting temperature due to elastic energy exceeds the difference between the melting temperature and solid−solid PT temperature and (b) plasticity and fracture are suppressed.

In particular, complex organic crystalline systems for which plasticity is suppressed (e.g., due to a large Burgers vector) and polymorphs that are connected by reconstructive PT with large transformation strain, are good candidates. If the pressure−temperature phase diagram contains the triple (1−2−m) point (Figure 8), then a change in pressure, which makes θ_{1-2} and θ_{2-m} closer, will render virtual melting the leading mechanism of a solid−solid PT for the majority of material systems with suppressed plasticity. Also, alloying may change the relationships between θ_{1-2} and θ_{2-m} and can also promote virtual melting.

An alternative mechanism of stress relaxation during melt crystallization is an amorphization. A nanometer-sized amorphous layer was observed for PTs from cubic BN to hexagonal BN and back ($\epsilon_0 = 0.53$) near the triple point.[35] It was not explained in ref 35 by any known reason but was explained in our letter[14] by virtual melting. The authors of ref 35 agreed that the explanation is plausible.[36]

Note that in our recent letter,[37] the virtual melting mechanism was expanded to the broad class of pressure-induced crystal−crystal and crystal−amorphous PTs. They occur in materials with the specific pressure−temperature phase diagram when the melting temperature of one of the phases reduces with growing pressure. The transformation path, considered in ref 37, is $1_{\text{stressed}} \rightarrow \text{VM1} \rightarrow 2_{\text{amorphous}}$, where the stressed phase 1_{stressed} is around the stressed crystalline nucleus of phase 2 which appears inside the matrix of phase 1. This transformation path is completely different from the one considered here, which results in completely different thermodynamics and kinetics. Our theory was applied for a new interpretation of melting, crystal−crystal, and crystal−amorphous PTs mechanisms in ice I_h. A similar mechanism is expected in amorphization of α quartz, coesite, jadeite, polymet, Ge and Si, BN, and graphite. Note that amorphization and consequently virtual melting in Si and Ge occur at more than 1000 K below the thermodynamic melting temperature at the same pressure!

Each known mechanism of solid−solid PT, stress relaxation, and loss of coherency (the generation of perfect and partial dislocations and fracture) is under intensive experimental (e.g., TEM, HRTEM, X-ray with synchrotron radiation, FTIR, and Raman methods) and theoretical (e.g., molecular dynamics, phase field, discrete dislocation, and mesoscopic continuum mechanic approaches) study. We expect the same to happen with this mechanism, definitely for HMX. HMX is an important explosive currently with wide applications and broad interest, which is under intensive study in governmental and academic laboratories. Other direction of future research is the search for material systems and conditions for which this mechanism can be found. The equations obtained will direct such a search, in particular, near triple points on the phase diagram. We believe that there are experimental data for a number of materials that can be interpreted using the virtual melting mechanism, similar to what has occurred with HMX crystals. Note that the virtual melting mechanism simplifies significantly the thermodynamic and kinetic model for the large-scale simulation of $\beta \leftrightarrow \delta$ PTs in the HMX crystals which are currently under development.[26]

Surface premelting attracted a great deal of interest.[16] Perhaps virtual surface melting, for which reduction in the melting temperature is much larger and which can lead to loss of coherency of epitaxial films and to alternative surface phases, will also be of interest. We hope this paper will attract general interest in connecting surface and bulk phenomena. We also mention that the solid−solid p6 → p3 PT between two 2D phases of annexin 5 (a soluble protein) starts via local melting at the grain boundaries of the p6 phase.[38]

Note that it is found in the monograph[39] that solid−solid PTs for a variety of organic materials look like crystallization of the product phase from the medium of the parent phase, very much like that from a liquid. Perhaps virtual melting also contributes to this phenomenon. Finally, methods can be designed to synthesize hidden metastable phases which cannot appear without virtual melting.

Acknowledgment. V.I.L. acknowledges the support of the NSF (CMS) and LANL (13720-001-05-AH). B.F.H., L.B.S., and B.W.A. acknowledge the support of the Laboratory Directed Research and Development and H.E. Science Programs at Los Alamos National Laboratory. This work has been completed during V.I.L.'s sabbatical leave at LANL. The hospitality of L.B.S., B.F.H., and B.W.A. is very much appreciated.

References and Notes

(1) Wayman, C. M. *Introduction to the Crystallography of Martensitic Transformation*; Macmillan: New York, 1964.

(2) Christian, J. W. *The Theory of Transformation in Metals and Alloys*; Pergamon Press: Oxford, U.K., 1965.

(3) Porter, D. A.; Easterling, K. E. *Phase Transformations in Metals and Alloys*; Van Nostrand Reinhold (International): London, 1989.

(4) Olson, G. B.; Cohen, M. Dislocation Theory of Martensitic Transformations. In *Dislocations in Solids*; Nabarro, F. R. N., Ed.; Elsevier Science Publishers B V: New York, 1986; Vol. 7, pp 297−407.

(5) Grinfeld, M. A. *Thermodynamic Methods in the Theory of Heterogeneous Systems*; Longman: Sussex, U.K., 1991.

(6) Levitas, V. I. Parts I and II. *Int. J. Plast.* **2000**, *16*, 805 and 851.

(7) Levitas, V. I. *Int. J. Solids Struct.* **1998**, *35*, 889.

(8) Levitas, V. I. Continuum Mechanical Fundamentals of Mechanochemistry. In *High-Pressure Surface Science and Engineering*; Gogotsi, Y., Domnich, V., Eds.; Institute of Physics: Bristol, U.K., 2004; pp 159−292.

(9) Levitas, V. I.; Preston, D. L. *Phys. Rev. B* **2002**, *66*, 134207.

(10) Henson, B. F.; Smilowitz, L. B.; Asay, B. W.; Dickson, P. M. *J. Chem. Phy.* **2002**, *117*, 3780.

(11) Smilowitz, L. B.; Henson, B. F.; Asay, B. W.; Dickson, P. M. *J.Chem. Phys.* **2002**, *117*, 3789.

(12) Burnham, A. K.; Weese, R. K.; Weeks, B. L. *J. Phys. Chem. B* **2004**, *108*, 19432.

(13) Cady, H. H.; Smith, L. C. *Studies on the Polymorphs of the HMX*; LAMS-2652, 1962. Cady, H. H. In *Analyses of Propellants and Explosives*; 17th International Annual Conference of ICT; Karlsruhe, Germany, 1986; pp 17.1−17.12.

(14) Levitas, V. I.; Henson, B. F.; Smilowitz, L. B.; Asay, B. W. *Phys. Rev. Lett.* **2004**, *92*, 235702.

(15) Levitas, V. I.; Smilowitz, L. B.; Henson, B. F.; Asay, B. W. *Appl. Rev. Lett.* **2005**, *87*, 191907.

(16) Henson, B. F.; Robinson, J. M. *Phys. Rev. Lett.* **2004**, *92*, 246107.

(17) Mura, T. *Micromechanics of Defects in Solids*; Martinus Nijhoff Publ.: Dordrecht, The Netherlands, 1987.

(18) Bukhovski, A. D.; Gelmont, B. L.; Shur, M. S. *J. Appl. Phys.* **1995**, *78*, 3691.

(19) Roitburd, A. L. *Phase Transitions* **1993**, *45*, 1.

(20) Brill, T. B.; Karpowicz, R. J. *J. Phys. Chem.* **1982**, *86*, 4260.

(21) Herrmann, M.; Engel, W.; Eisenreich, N. *Propellants, Explos., Pyrotech.* **1992**, *17*, 190.

(22) Lyman, J. L.; Liau, Y. C.; Brand, H. V. *Combustion Flame* **2002**, *130*, 185.

(23) Menikoff, R.; Sewell, T. D. *Combust. Theory Modell.* **2002**, *6*, 103.

(24) Sewell, T. D.; Menikoff, R.; Bedrov, D.; Smith, G. D. *J. Chem. Phys.* **2003**, *119*, 7417.

(25) Henson, B. F.; Asay, B. W.; Sander, R. K.; Son, S. F.; Robinson, J. M.; Dickson, P. M. *Phys. Rev. Lett.* **1999**, *82*, 1213.

(26) Levitas, V. I.; Smilowitz, L. B.; Henson, B. F.; Asay, B. W. *J. Chem. Phys.* **2006**, *124*, 026101.

(27) Landers, A. G.; Brill, T. B. *J. Phys. Chem.* **1980**, *84*, 3573.

(28) Smilowitz, L. B.; Henson, B. F.; Greenfield, M.; Sas, A.; Asay, B. W.; Dickson, P. M. *J. Chem. Phys.* **2004**, *121*, 5550.

(29) Teetsov, A. S.; McCrone, W. C. *Microsc. Cryst. Front* **1965**, *15*, 13.

(30) Levitas, V. I.; Idesman, A. V.; Olson, G. B.; Stein, E. *Philos. Mag. A* **2002**, *82*, 429.

(31) Weeks, B. L.; Ruddle, C. M.; Zaug, J. M.; Cook, D. J. *Ultramicroscopy* **2002**, *93*, 19.

(32) Hill, R. *Mathematical Theory of Plasticity*; Clarendon Press: Oxford, U.K., 1950.

(33) Weese, R. K.; Burnham, A. K. *Propellants, Explos., Pyrotech.* **2005**, *30*, 344.

(34) Levitas, V. I. *Phys. Rev. B* **2004**, *70*, 184118.

(35) Eremets, M. I.; Takemura, K.; et al. *Phys. Rev. B* **1998**, *57*, 5655.

(36) Eremets, M. I.; Gavriliuk, A. G.; Serebryanaya, N. R.; Trojan, I. A.; Dzivenko, D. A.; Boehler, R.; Mao, H. K.; Hemley, R. J. *J. Chem. Phys.* **2004**, *121*, 11296−300.

(37) Levitas, V. I. *Phys. Rev. Lett.* **2005**, *95*, 075701.
(38) Reviakine, I.; Bergsma-Schutter, W.; Morozov, A. N.; Brisson, A. *Langmuir* **2001**, *17*, 1680.
(39) Mnyukh, Y. *Fundamentals of Solid-State Phase Transitions, Ferromagnetism and Ferroelectricity*; 1st Books Library, www.1stbooks.com.